DrJes

Dawson Research Journal of Experimental Science

Winter 2019

Volume 14

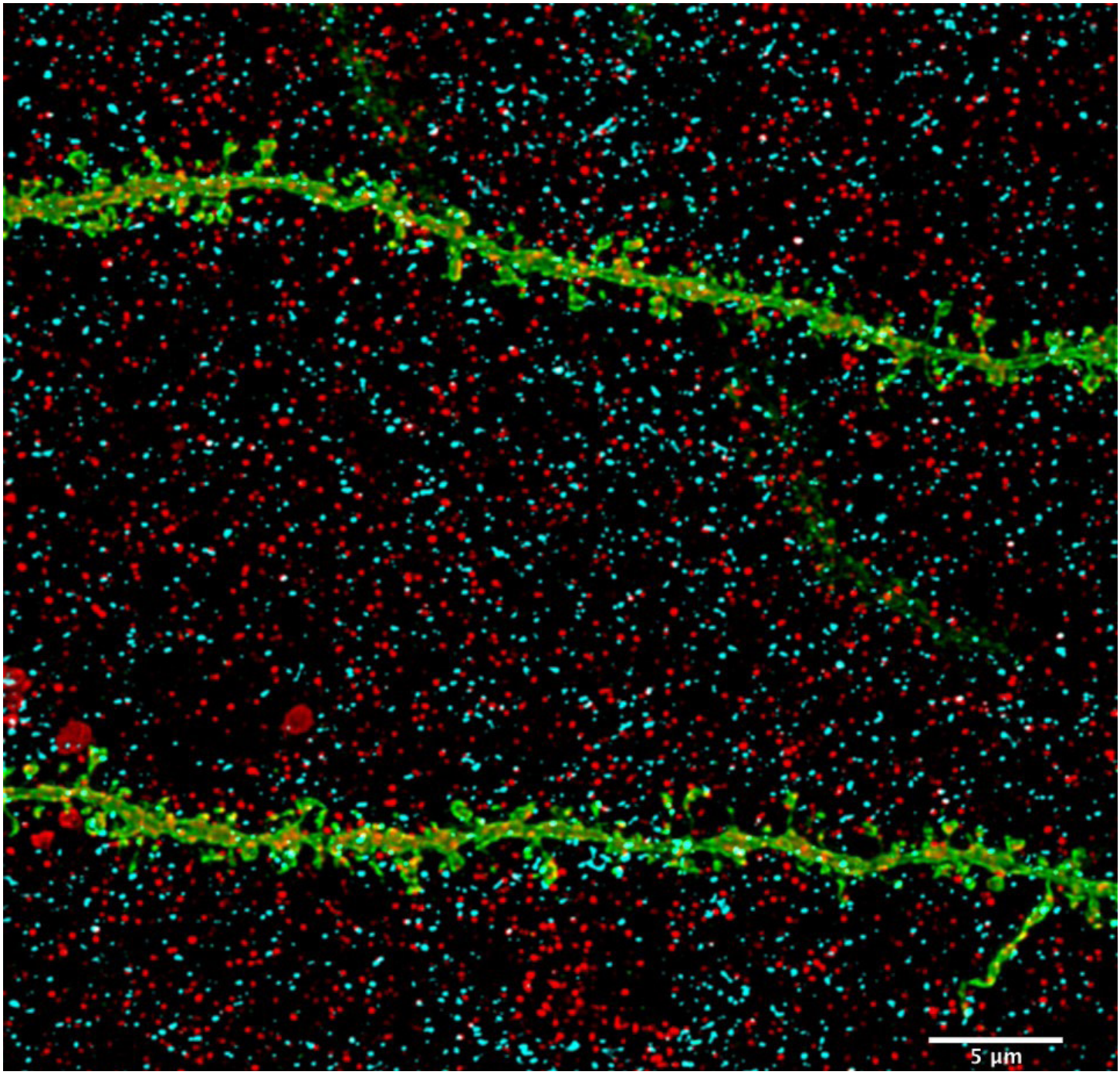

Features

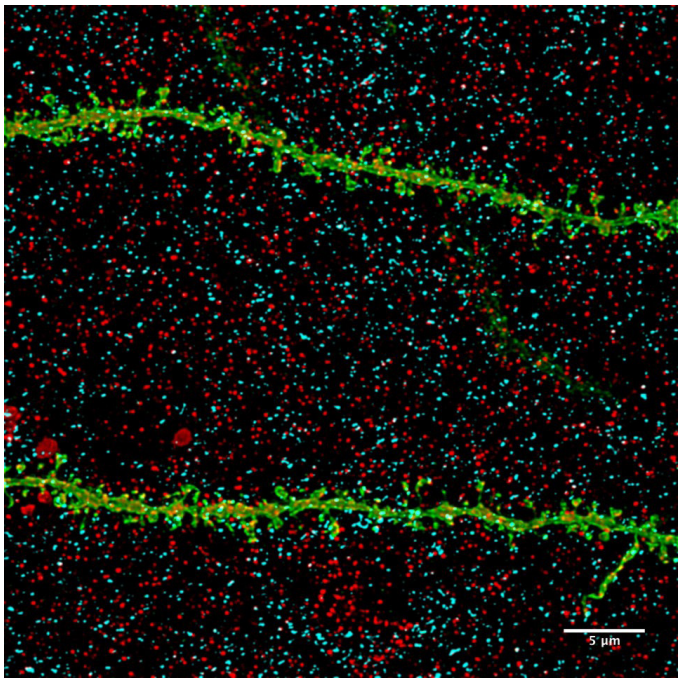

About the Cover

The image shows immunohistochemical staining of a tissue section from an adult mouse hippocampus, a structure in the brain critical for the formation of new memories. Two dendrites of hippocampal neurons are labelled green with GFP (Green Florescent Protein). Many post-synaptic specializations called dendritic spines protrude from each of the two labelled dendritic shafts. Dendritic spines are thought to change shape and function when new memories are formed. The distribution of a pre-synaptic protein is labeled cyan and a post-synaptic protein red. Many more dendrites are present in the image, consistent with the hundreds of synaptic markers throughout the image, but only two dendrites are labelled green, which allows the detailed dendritic structure to be visualized. The scale bar in the lower right corner corresponds to 5 microns, or 1/200 of a millimeter. A typical synapse is less than 1 micron in diameter, or less than 1/1000 of a millimeter. A human brain is thought to contain ~1 x 10e15 synapses. Imaging by Dr. Stephen Glasgow and Professor Tim Kennedy, using laser scanning confocal super-resolution microscopy, Montreal Neurological Institute, McGill University.

Letter from the Editors

We are proud to present the 14th volume of DrJes. This volume is a collection of our fellow students' comprehensive examinations and independent study research projects. This journal, over the past 20 years, has created a place for students to share their hard work and accomplishments with the Dawson community.

From day one, our mission was to provide students with an opportunity to publish their work but also receive incredible feedback from not only the editors but professionals in different fields of study. Whether it is a research paper in biology or particle physics, an expert in that field from universities and CEGEPs in Quebec, New Brunswick, and Ontario have given their stamp of approval and helpful feedback on all articles present in this journal.

We want to take this opportunity to thank everyone who has gone the extra mile to present this journal to you. Our incredible authors who have written papers concerning their interests in varying scientific fields and the editors whom week by week combed through the articles correcting and providing authors with feedback have all been valuable in presenting this journal. It was a pleasure working with all of you, and we would like to wish you the best in your future endeavours. Understanding the time and effort put into every one of these articles from start to finish, we hope you take the time to read these articles and appreciate the greatness of their work.

Finally, we would like to once again thank our extraordinarily committed and hard-working editors for their fantastic work on all of the papers. We would also like to give immense thanks to our advisors, Jaleel Ali and Brid Nic Nicoaill for their continuous guidance and support during the making of this year's version of DrJes as this journal would not be possible without you!

We hope you enjoy this issue!

Tyler Baum, Hayley Mendel, and Evan Puligandla

Co-Editors-in-Chief, 2018-2019

The Editorial Board gratefully acknowledges the financial support provided by Dawson College's Office of Academic Development that made this publication possible.

Contents

The Quantitative Effects of Benzalkonium Chloride-based Disinfectants on Bacterial Growth and Pathogenic Cross-contamination

Ryan M. Knobovitch and Kasra Tehranimehr

Abstract

Prokaryotic microorganisms can maintain positive ecological relationships, but they can also have pathogenic properties which can result in diseases and infections, making proper hand hygiene an ongoing worldwide concern. Aiming to maximize the efficiency of such a task, the purpose of this research project was to experimentally determine whether a Benzalkonium chloride (BZK) based antibacterial soap was more effective than a standard liquid hand soap at inhibiting bacterial growth and preventing pathogenic cross-contamination.

Hand swab samples were isolated from ten different individuals, half of whom washed their hands with BZK-based antibacterial hand soap and the other half with standard liquid hand soap. After a 48-hour incubation period, the quantity of bacterial growth present in the BZK samples and that of the generic liquid hand soap samples were compared. A p-value with an alpha that was highly statistically significant was obtained.

In today's world where new bacterial strains are being discovered, and pre-existing ones are continually mutating, these results are not only significant but both scientifically and clinically relevant. Knowing which product is most effective, gives members of the public the information needed to enforce and follow proper infection control measures.

Introduction

This research project was intended to experimentally discover whether an antibacterial hand soap containing BZK is more effective at inhibiting bacterial growth than generic liquid hand soap. The hypothesis is that antibacterial soap containing BZK will be more effective at inhibiting bacterial growth than generic liquid hand soap and will, therefore, produce a lower quantitative value of bacterial colonies. That said, there are typically 40 million bacterial cells in a single gram of soil and a million bacterial cells in a milliliter of fresh water (Gargaud M., 2011). Knowing which hygiene products are both efficient and effective offers the public applicable information on how to decrease the spread of pathogenic bacteria, reduce risks of infection and promote global health. Proper hand hygiene is recognized as one of the most crucial steps in preventing the spread of pathogens and the cross-contamination of bacteria among individuals, foods, and surfaces (CDC, 2015). Liquid hand soap has been publicly available for over 150 years. However, antibacterial soaps have since been shown to have more success in inhibiting bacterial growth.

Antibacterial soaps differ from generic liquid hand soaps by the presence of a chemical compound that is proven to inhibit the growth of bacteria. Since the 1960s, the most widely used antibacterial chemical has been Triclosan, a poly-chloro phenoxy phenol which is a type of organic polyhalogenated compound (Rule KL et al., 2005). Despite its commercial use that has spanned over five decades, in 2016, the United States Food and Drug Administration (FDA) issued a final rule on safety and effectiveness of Triclosan, removing it from over-the-counter antibacterial hand and body washes (U.S. Food & Drug Administration, 2016). Soon after the FDA's announcement, many companies started to replace Triclosan with other antibacterial compounds – BZK (Benzalkonium chloride) being the leading alternative (Kodjak A., 2016).

BZK is an organic salt, classified as a quaternary ammonium compound (QAC) and a non-alcohol based antibacterial chemical used for clinical, food line and domestic household biocides (Mangalappalli-Illathu, A. K. et al., 2006). QACs like BZK are commonly used as antibacterial agents due to their cationic amphiphilic properties. BZK's hydrophilic cationic region destabilizes a pathogen's surface by forming electrostatic interactions with negatively charged components. After the destabilization occurs, BZK's antiseptic properties cause denaturation of the pathogens' proteins and cause lysis of the cytoplasmic membrane (Ittoop, S. M. et al., 2015). The ultimate effects of BZK are membrane destruction and disruption of essential cell processes including ATP synthesis and solute uptake (McDonnell, G. et al., 1999).

BZK's antibacterial activity is most effective against Gram-positive bacteria, along with some Gram-negative bacteria, enveloped viruses, fungi, and protozoa (Fazlara, A. et al., 2012). Staphylococcus aureus and Enterococcus spp. are both gram-positive bacteria, and established pathogens in the hospital environment. Their frequent multidrug resistance often complicates therapy but can be eradicated by agents such as BZK before invading a host and causing an infection. In 2013, 176 acute-care hospitals within Canada were surveyed and found that on any given day about 1 in 12 Canadian adults in hospitals are either colonized or infected with a superbug which are strains of bacteria that are resistant to most common antibiotics (The Canadian Press, 2013). These superbugs were derived from MRSA (methicillin-resistant Staphylococcus aureus), VRE (vancomycin-resistant Enterococci) and Clostridium difficile – all of which are Gram-positive bacteria. Researchers found that there were lower prevalence rates of infection in hospitals that had stronger policies for sanitation and disinfection. Staphylococcus aureus, for example, can survive on antisep-

tic-free hands for up to 150 minutes, which is enough time for it to spread and cause nosocomial infections (Kampf, G. et al., 2004). Handwashing with an antibacterial soap containing BZK would readily kill the bacteria, whose cell walls are mainly composed of slightly negatively charged peptidoglycan and teichoic acids that may present in hospitals and other shared spaces if otherwise.

Antibacterial compounds work through one of two possible property pathways: They are either bacteriostatic, which stops bacterial reproduction without necessarily killing the cells, or bactericidal, which causes immediate cell death. BZK, which has predominantly bacteriostatic properties, was often considered inferior to a compound such as Triclosan, which is strictly bactericidal (McDonnell, G. et al., 1999). However, in Clinical Relevance of Bacteriostatic versus Bactericidal Mechanisms of Action in the Treatment of Gram-Positive Bacterial Infections, researchers set out to determine the distinction between a bacteriostatic and bactericidal agent and their antibacterial properties. The researchers determined that the presumption of the superiority of bactericidal action over bacteriostatic action in the treatment of gram-positive bacterial infections is intuitive rather than based on rigorous scientific research (Pankey, G.A. et al., 2014). Furthermore, the article supported that both properties were equally efficient in both preventing and treating an infection.

Concludingly, do antibacterial compounds like BZK actually make a difference in reducing disease and preventing the onset of infection, or do they pose a higher risk than they do reward regarding public consumer use?

*Materials and Method*s

The bacterial samples were inoculated on agar plates as a form of growth medium. The agar was made using 8 grams of agar powder from a nutrient agar kit by Seaweed Solution Laboratories which contained 21.7% Pancreatic Digest of Gelatin (Peptone G), 13% beef extract and 65.3% Agar. The nutrient agar was dissolved into 350 mL of distilled water and brought to a boil. The agar was evenly poured into ten sterile Petri dishes measuring 3.5 cm in diameter, with the depth of the agar in each Petri dish measuring 0.635 cm. The Petri dishes were kept at room temperature until the agar solidified. Using a permanent marker, each Petri dish was divided into three sections: The control, pre-washing, and post-washing (for both soaps respectively). Five of the Petri dishes were used to test the results of BZK, while the other five were used to test the generic liquid hand soap. The Petri dishes were then stored in a refrigerator at 2.1°C until the observers transported them to the site where the cultures were collected 21 hours later. The Petri dishes were carried in a cooler at 1.9°C.

The accessibility to such an environment by one of the observers, allowed the cultures to be collected from volunteers at an acute-care walk-in clinic. After accepting to participate in the study, ten randomly chosen participants were asked to deliberately touch the same high traffic contact surfaces throughout the clinic to collect similar strains of bacteria on their hands. Additionally, they were asked not to clean their hands with any soap or disinfectant for fifteen minutes.

Using a predetermined random sequence unknown to the participants, half of the participants were asked to wash their hands with an antibacterial liquid hand soap containing 0.13% BZK (Softsoap Antibacterial liquid hand soap). The other half of the participants were asked to wash their hands with generic liquid hand soap (Softsoap liquid hand soap). Each individual was carefully instructed to lather the backs of both hands, between all ten fingers and under the nails. They were asked to perform these instructions for no less than 20 seconds, which is the hand washing standard set by the Centers for Disease Control and Prevention (CDC, 2016). Each participant was provided with their own sealed bottle of 250 mL of distilled water for rinsing, along with a piece of paper towel to dry their hands to ensure control variables were followed correctly.

A sterile cotton swab soaked in distilled water was then wiped between the fingers and across the palm of the dominant hand of each participant. In the presence of an open flame from two nearby candles that helped produce a sterile environment during culturing the swabs were then used to inoculate a bacterial lawn in the appropriate sections of each Petri dish. This step was also performed pre-washing, to compare with the BZK results post-incubation. All ten Petri dishes were sealed with Parafilm to minimize the bacterial mediums from being contaminated by airborne pathogens during incubation. The Petri dishes were then stored in a transport case at room temperature for 48 hours before being examined. The transport case did not permit the entrance of light and overall, was considered to be an environment that would promote bacterial growth.

The data was analyzed 48 hours after incubation, and the colony morphology from each Petri dish was recorded and consolidated into both a table and a graph as shown below (Figure 1, Table 1). A t-test was used to determine whether or not there was a significant statistical difference, which allowed the observers to conclude whether to reject or fail to reject the null hypothesis.

Results

The average number of colonies grown from the cultures collected from participants who washed their hands with the antibacterial versus generic hand soap was 5.4 and 38.2 respectively. There was zero bacterial growth in the control groups, which supported that the aseptic technique was followed correctly and that there was no cross-contamination in the cultures. For individual analysis, the average number of colonies grown in the pre-washing sections for all ten participants averaged approximately 90 bacterial colonies, calculated via standard deviation, and differed vastly in colony

morphology. Comparing the bacterial growth after incubation, BZK hindered 94% of the potential growth, versus the generic liquid hand soap which only inhibited 58%. Given the environment from which the participants were chosen, these percentage values supported a high likelihood that the bacterial strains collected were to some extent resistant to generic liquid hand soap.

From these results, it was concluded that regarding a quantitative value, the BZK based antibacterial liquid hand soap grew 86% less bacterial colonies than generic liquid hand soap. The p-value of less than 0.0001 (Appendix), which is an alpha value of less than 0.05, signifies that the difference between the means is exceptionally significant (Table 1). Analysis of the data shows that when BZK based antibacterial soap is used in conjunction with proper hand hygiene techniques, the number of bacterial colonies grown is significantly reduced than when washing with generic liquid hand soap. The generic liquid hand soap's number of bacterial colonies ranged from 32 to 44 and included six different bacterial species. The antibacterial liquid hand soap's number of bacterial colonies ranged from 4 to 7 and included two different bacterial species. The antibacterial liquid hand soap yielded the lowest amount of bacterial growth. Statistically, the observers were able to reject the null hypothesis on the basis that the p-value and t-test supported the alternative hypothesis as the results rendered an alpha that was less than 0.05.

Upon analyzing colony morphology, it is evident that there was a significant difference in the physical characteristics of bacterial growth when comparing the two sample groups. Generic liquid hand soap had much more diversity in colors, textures, and degree of light reflection, whereas antibacterial liquid hand soap was selective to only a handful of characteristics. Except for participant H, whose colonies were white, the physical characteristics (Table 2) of all other sections of bacterial growth from participants who washed their hands with antibacterial liquid hand soap were physically identical to the naked eye. The hypothesis behind this finding was that the bacteria grown in each sample of antibacterial soap was most likely of the same or closely related species that were not affected by BZK's antibacterial properties.

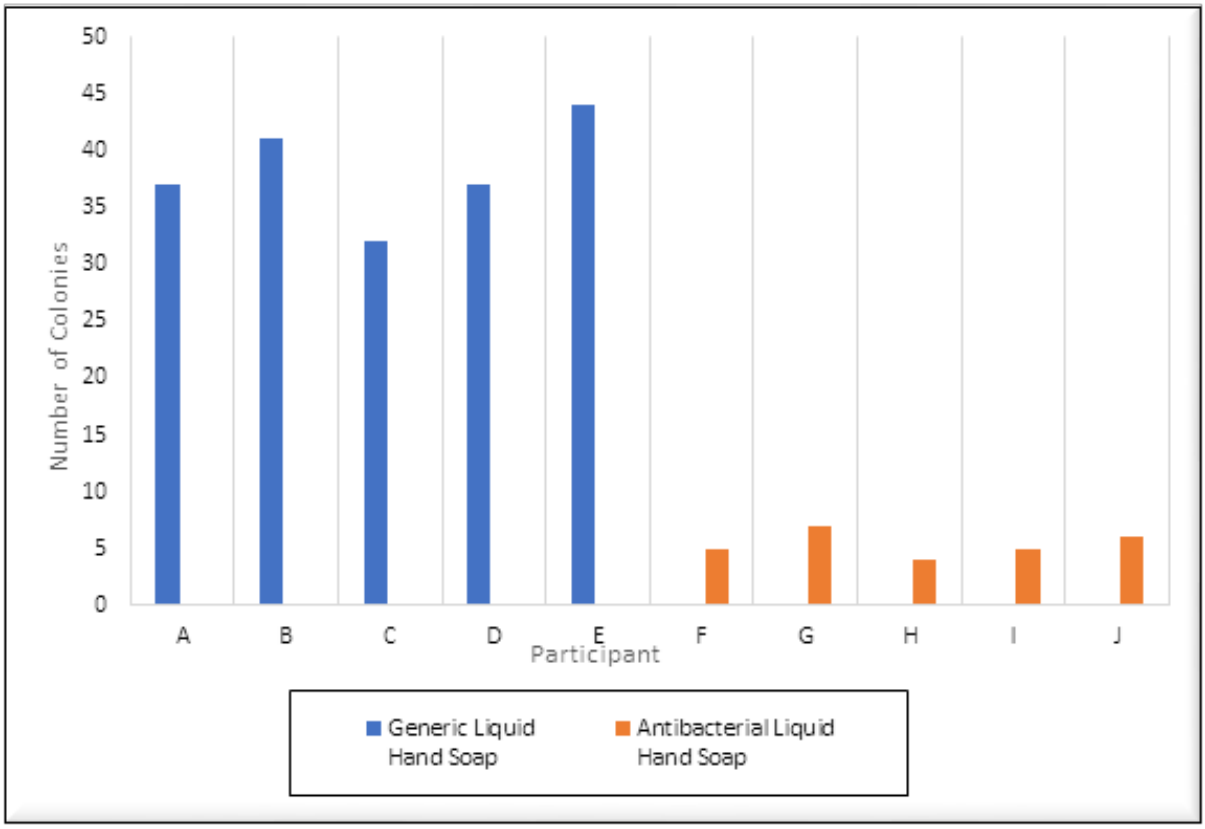

Figure 1: Number of Bacterial Colonies Grown from Ten Different Study Participants

Each bar represents a quantitative value of the bacterial colonies grown in each respective section from each Petri dish. Omission of representing the control group in the figure above is a result of having no bacterial growth in said group.

Type of Soap	Mean (s)	Variance (S^2)	Standard Deviation (s)	P-Value	Degree of Freedom	Sample Size (n)
Generic Liquid Hand Soap	38.2	20.7	4.54	< 0.0001	8	5
Antibacterial Liquid Hand Soap	5.4	1.3	1.14			5

Table 1: Descriptive and Inferential Results of BZK Based Antibacterial Liquid Hand Soap Versus Generic Liquid Hand Soap

	Number of bacterial colonies	Number of Bacterial Species	Colony Color	Colony Shape	Colony Texture	Light Reflection of Colony	Transparency of Colony
Participant A	37	4	white + tan	circular	smooth	glossy	opaque
Participant B	41	6	white + beige	circular	smooth	glossy	opaque
Participant C	32	5	white	circular	smooth + rough	glossy + matte	opaque
Participant D	37	4	white + tan	circular	smooth + rough	glossy + matte	opaque
Participant E	44	5	white + tan	circular	smooth + rough	glossy	opaque
Participant F	5	1	tan	circular	smooth	glossy	opaque
Participant G	7	2	tan	circular	smooth	glossy	opaque
Participant H	4	1	white	circular	smooth	glossy	opaque
Participant I	5	1	tan	circular	smooth	glossy	opaque
Participant J	6	2	tan	circular	smooth	glossy	opaque

Table 2: ***Colony Morphology of Bacterial Growth Results of BZK based Antibacterial Liquid Hand Soap versus Generic Liquid Hand Soap*** **Participants A through E (blue) washed their hands with generic liquid hand soap. Participants F through J (orange) washed their hands with a BZK based antibacterial liquid hand soap.**

Discussion

With the recorded results which demonstrated a p-value (Table 1) less than 0.0001, it was concluded that regarding this particular study, the BZK based antibacterial soap had the most significant effect on hindering bacterial growth on the hands of the participants that partook in the experiment. The results support the hypothesis that BZK provides stronger quantitative results when compared to those of generic liquid hand soap. In light of the calculated p-value, this study supports the rejection of the null hypothesis and subsequently confirms that the BZK based antibacterial soap sections do statistically have lower amounts of bacterial growth than those of the generic liquid hand soap.

Although the results collected supported both the experimental and statistical hypotheses, other measures could have been taken to improve the quality of the study. The observers could have completed more trials with different participants at more than one location to determine if any of those factors influenced the results. Furthermore, being able to test different BZK based products such as antiseptic sprays and hand sanitizers, may have provided interesting results for comparison purposes.

Noteworthy, the observers were also limited in their available resources throughout the experiment, and as such, it was not possible to investigate the bacterial growth further than colony morphology. If this experiment were to be redone in the future, the observers would examine the cultures at a microscopic level to determine the type of bacterial species that were grown. Moreover, a gram stain test would be performed to determine whether the bacteria were grown was Gram-positive or Gram-negative, which would also contribute to determining the type of bacterial species.

References

1. Gargaud, M., Amils, R., James Cleaves, H. (2011). *Encyclopedia of Astrobiology,* Springer-Verlag Berlin Heidelberg. p. 137.
2. CDC – Centers for Disease Control and Prevention (2015). *Handwashing: Clean Hands Save Lives.* Publications, Data & Statistics. US Department of Health & Human Services.
3. Rule, K.L., Ebbett, V.R., Vikesland, P.J. (2005). *Formation of chloroform and chlorinated organics by free-chlorine-mediated oxidation of Triclosan*. Environ. Sci. Technol. Issue 39, p. 76–85
4. Fischer, A., Office of the Commissioner, United States Food and Drug Administration (2016). *Press Announcements – FDA issues final rule on safety and effectiveness of antibacterial soaps*.
5. Kodjak, A., Health News, National Public Radio (2016). *FDA Bans 19 Chemicals Used in Antibacterial Soaps*.
6. Mangalappalli-Illathu, A.K., Korber, D.R. (2006). *Adaptive resistance and differential protein expression on Salmonella enteric serovar enteritidis biofilms exposed to Benzalkonium chloride*. Antimicrobial agents and chemotherapy, Issue 50, p. 3588-3596.
7. ttoop, S.M., Seibold, L.K., Kahook, M.Y., (2015). *Ocular Surface Disease and the Role of Preservatives in Glaucoma Medications*. Glaucoma, Second Edition, p. 593-597.
8. McDonnell, G., Russell, A.D. (1999). *Antiseptics and disinfectants: activity, action, and resistance*. Clinical Microbiology Reviews, 12 (1): 147-179.
9. Fazlara, A., Ekhtelat, M. (2012). *The disinfectant effects of Benzalkonium chloride on some important foodborne pathogens*. American-Eurasian Journal of Agricultural & Environmental Science, Issue 12, p. 23-29.
10. The Canadian Press, CBC News (2013). *1 in 12 Canadian adults in hospital have superbug: study. Survey of 176 acute-care hospitals looked at MRSA, VRE and C. difficile*.
11. Kampf, G., and Kramer, A. (2004). *Epidemiologic background of hand hygiene and evaluation of the most important agents for scrubs and rubs*. Clinical Microbiology Reviews, Issue 4, p. 863-893
12. Pankey, G.A., and Sabath, L.D., US National Library of Medicine. National Institutes of Health (2014). *Clinical Relevance of Bacteriostatic versus Bactericidal Mechanisms of Action in the Treatment of Gram-Positive Bacterial Infections.*
13. CDC – Centers for Disease Control and Prevention (2016). *Handwashing: Clean Hands Save Lives.* US Department of Health & Human Services.
14. Graph Pad Software (2017). *QuickCalcs: T test calculator.*

Ghosts and Tachyons in Transparent Branes

Samuel Fisher, Jonah Saks, Simon Lapointe, Manuel Toharia, and Aidan Zentner

Abstract

We consider general models with one compact extra dimension in which fields are defined with the usual 5d Lagrangian within the bulk of the extra dimension, but with the addition of kinetic terms localized at the boundaries. We show that when the coefficients of these brane kinetic terms have the wrong sign, the effective 4d theory emerging from the setup presents instabilities in the form of tachyons or ghosts. We carefully show this for the case of a scalar field in a flat extra dimension with no mass terms. The result should be extensive to particles of any spin (including gravitons), and for any warping of the metric along the extra dimension, including when bulk mass terms are considered.

Introduction

The standard model of particle physics is a theory that has been incredibly successful in explaining many parts of our universe, from the properties of elementary particles to the description of three of the four fundamental forces. However, for all of its success, there remain many fundamental mysteries about our universe that the standard model simply cannot explain. An example that is of particular interest to this paper is the failure to explain the large discrepancy in strength between gravity and the [i] weak nuclear force, known as the hierarchy problem. Our understanding of the quantum world is incomplete, and in order to gain a full understanding of our universe, we must go beyond the standard model.

For decades, the idea of extra spatial dimensions has been at the heart of many theories that hold incredible promise of solving some of these mysteries [1–8]. In these theories, our universe does not end with the four-dimensional world that we inhabit, but extends into other dimensions, where the particles that we see around us may exist. Our perception of these particles could therefore be a result of their behaviour in these extra dimensions.

What would a particle look like in this dimension? We can imagine this extra dimension as a two close sheets, and the particles as waves that oscillate across the gap between these sheets, which corresponds to the width of the dimension. For every width that could be taken on, we can imagine a discrete set of particles that can exist across it. This is the case because only those particles that oscillate with frequencies that create a standing wave across the dimension can be physical particles. Each standing wave exhibits different behaviour, and this changes the way we perceive it in our four-dimensional world.

In this paper, we focus on adding kinetic terms to the boundaries of the extra dimension [9–11]. These terms are kinetic energy that changes the behaviour of the particle oscillations. As these kinetic terms are pushed to negative values, inconsistencies emerge in the model in the form of tachyons particles with imaginary mass, and ghosts, states of the field with negative probability

5D Scalar with Brane Potential and Brane Kinetie Energy

Let's consider a sector of a 5D scenario with a real scalar field $h(x,\ y)$ defined by the following action:

$$S = \int d^4x dy \sqrt{g}\left(\left|D^M h\right|^2 - V\left(h\right)\right) + \sum_i \int d^4x dy \sqrt{g}\delta\left(y - y_i\right)\left(d_i\left|D^M h\right|^2 - \lambda_i\left(h\right)\right) \tag{1}$$

The fifth dimension is understood as an interval, with the boundary terms fixing the boundary conditions of the fields.

The background spacetime metric is assumed to be the extra dimensional extension of the flat Minkowski metric,

i.e., $ds^2 = \eta_{\mu\nu}dx^\mu dx^\nu - dy^2$ (2)

where the signature is $(+,\ -,\ -,\ -,\ -)$. The Euler-Lagrange equation for the real perturbations $h(x,\ y)$ in the bulk is

$$\partial_\mu \partial^\mu h - h'' + \left.\frac{\partial^2 V}{\partial h^2}\right|_{h=0} h = 0 \tag{3}$$

with the jump conditions on h

$$d_i \partial_\mu \partial^\mu h + \left(\left.\frac{\partial^2 \lambda_i}{\partial h^2}\right|_{h=0}\right) h\Big|_{y=y_i} = \left[h'\right]_{y_i} \tag{4}$$

We can now separate variables on $h(x,\ y)$ and write $h(x,\ y) = h_x(x)h_y(y)$. Upon separation, equation (3) leads to the system

$$\partial_\mu \partial^\mu h_x + m_{h_n}^2 h_x = 0 \tag{5}$$

$$h_y'' - \left(\mu_V^2 - m_{h_n}^2\right) h_y = 0 \tag{6}$$

with $\mu_V^2 = \left.\frac{\partial^2 V}{\partial h^2}\right|_{h=0}$ and where the jump conditions on h_y'

$$\left(\mu_{\lambda_i}^2 + m_{h_n}^2 d_i\right) h\Big|_{y=y_i} = \left[h'\right]_{y_i} \tag{7}$$

with $\mu_{\lambda_i}^2 = \left.\frac{\partial^2 \lambda_i}{\partial h^2}\right|_{h=0}$ and where $m_{h_n}^2$ is the separationcon

stant. We can see that $m_{h_n}^2$ also plays the role of the mass term of a 4D particle as seen in in Eq. (5). Because there is an infinite but discrete set of possible values for $m_{h_n}^2$, we will say that the 5D compactified theory leads to a 4D effective theory containing an infinite tower of Kaluza-Klein (KK) scalar modes.

Solving (6) with the bulk mass term set to zero for simplicity ($\mu_V = 0$) we obtain

$$h_y = A\sin\left(m_{h_n} y\right) + B\cos\left(m_{h_n} y\right). \quad (8)$$

Without brane kinetic terms ($d = 0$) we can first look at two simple limits based on the brane localized masses (μ_{λ_i}).

- If we take the limit as the bulk mass becomes very large, the boundary conditions reduce to $h_{y_i} = 0$, that is to say, Dirichlet boundary conditions, and they yield, $h_y = A\sin\left(m_{h_n} y\right)$ (9)

  where $m_{h_n} = n\pi / y_1$ are the masses of the KK modes with $n = 1, 2, 3$ .... With the further normalization requirement that $\int_0^{y_1} h_y^2 dy = 1$, we find that $A = \pm\sqrt{2 / y_1}$.

- On the other hand, in the limit where the mass term and the brane kinetic term vanish, the boundary conditions become the Neumann conditions on the solution of (8), $\left[h'\right]_{y_i} = 0$, and we obtain

  $$h_y = B\cos\left(m_{h_n} y\right), \quad (10)$$

  where $m_{h_n} = n\pi / y_1$ and where $n = 1, 2, 3$ ... Again, requiring that $\int_0^{y_1} h_y^2 dy = 1$, yields $B = \pm\sqrt{2 / y_1}$.

In both cases we observe that the masses obtained for all the KK modes are all positive and thus the theory is well-behaved.

In order to simplify the study of the effect of the brane localized kinetic terms, we will allow such terms only on one of the boundaries (the one located at $y = y_1$) and thus we will set $d_0 = 0$ and $d_1 = d$. We will also set the brane masses to zero ($\mu_{\lambda_i} = 0$), and obtain a limit that we dub "transparent" branes because in this limit the boundary conditions are Neumann, and thus have a less drastic effect than if they were Dirichlet (in which case the fields would vanish on the boundary creating "opaque" branes). Because on the boundary located at $y = 0$, we do not have a mass term or a brane kinetic term, the boundary condition is Neumann at that brane, and thus we obtain the solution

$$h_y = \cos\left(\sqrt{m_{h_n}^2}\, y\right). \quad (11)$$

Imposing the boundary conditions in (7) on the bulk, the following equation is obtainedthat defines $m_{h_n}^2$:

$$d m_{h_n}^2 \cos\left(\sqrt{m_{h_n}^2}\, y_1\right) + \sqrt{m_{h_n}^2}\sin\left(\sqrt{m_{h_n}^2}\, y_1\right) = 0 \quad (12)$$

When the mass eigenvalues are small compared to the inverse scale y_1 (i.e., $\left(m_{h_n} y_1\right) << 1$, the previous equation can be expanded in powers of the small parameter $\left(m_{h_n} y_1\right)$ as

$$m_{h_n}^2\left(d + y_1 - \frac{m_{h_n}^2 y_1^2}{6}\left(3d + y_1\right)\right) + \mathcal{O}\left(\left(m_{h_n} y_1\right)^6\right) = 0 \quad (13)$$

and thus we find that there is always a zero mass solution, but also that a second small mass solution is possible with

$$m_{h_n}^2 = 6\frac{y_1 + d}{y_1^2\left(3d + y_1\right)} \quad (14)$$

where $(y_1 + d)$ must be small in order for the mass eigenvalue to be small (and thus the denominator cannot vanish or change sign in this approximation).

- If the brane kinetic term is positive ($d > 0$) the term $(y_1 + d)$ cannot be (parametrically) small and thus no second light solution exists.
- If the brane kinetic term is negative ($d < 0$) then $(y_1 + d)$ can be small and we can have a second light solution. Moreover, this second light solution can be tachyonic (i.e., $m^2 < 0$) if the kinetic term coefficient is negative $d < 0$ and if $|d| < y_1$. Otherwise, if the kinetic term is more negative than $-y_1$, then there is no tachyon (although we will see that there is then a ghost!).

The numerical results for all the masses in the KK tower can be seen in Figure 1.

Normalization Equation Derivation from 5d Action

Starting from the 5d action (1), we assume the wave function is separable in x and y ($h = h_x h_y$), where x is the usual 4d coordinates and y is the coordinate of the extra dimension. Concentrating on the first term of the action, we extract any terms which could contribute to the 5d kinetic term

$$\int d^4x dy \left(h_y^2 \left(\partial_x h_x \right)^2 \right) \tag{15}$$

The only term contributing to the 4d kinetic term is then

$$\int dy h_y^2 \int d^4x \partial^\mu h_x \partial_\mu h_x \tag{16}$$

Turning to the brane-localized term in the action, we do the same and obtain

$$\sum_i \int dy d_i \delta\left(y - y_i\right) h_y^2 \int d^4x \partial^\mu h_x \partial_\mu h_x \tag{17}$$

Evaluating the integral containing the Dirac delta-function, the contribution to the 4D kinetic term coming from the branes becomes

$$\sum_i d_i \, h_y^2\Big|_{y_i} \int d^4x \partial^\mu h_x \partial_\mu h_x \tag{18}$$

The canonical normalization condition is therefore:

$$\int dy h_y^2 + \sum_i d_i \, h_y^2\Big|_{y_i} = \frac{1}{2} \tag{19}$$

We analyze the trivial solution to this equation, in the case where there is a brane kinetic term only at $y = y_1$ (we take $y_0 = 0$):

$$\int_0^{y_1} dy h_y^2 + d_1 h_{y_1}^2 = \frac{1}{2} \tag{20}$$

where the general solution

$h_y = A \sin\left(\sqrt{m^2} y\right) + B \cos\left(\sqrt{m^2} y\right)$ becomes a constant B

for very small mass $m_{h_n}^2 = 0$. In that limit, (20) becomes

$$B^2 \left(\int_0^{y_1} dy + d_1 \right) = \frac{1}{2} \tag{21}$$

where B^2 must be non-zero, real and positive. Integrating and solving for d_1 gives the following result:

$$B^2 \left(y_1 + d_1 \right) = \frac{1}{2} \tag{22}$$

For all $d_1 < -y_1$, the left hand term of eq. 20 becomes negative, and

$$B^2 < 0 \tag{23}$$

The conclusion is that exactly when the mass of the lightest KK mode turns from imaginary to real, the theory becomes unphysical because the kinetic term becomes negative and we obtain a ghost. Thus, the ghost regime begins at the precise point where the tachyon regime ends, and we conclude that for any negative value of d, the theory leads to instabilities (ghost or tachyonic).

Numerical Masses of KK Particles

We finally study numerically the masses of the KK modes emerging from the 5D theory, and plot them as a function of the brane kinetic coefficient d, in the special case where the brane and bulk masses vanishes $\mu_V^2 = \mu_{\lambda_i}^2 = 0$ and taking the length scale to be $y_1 = 1$.

Notice that the tachyon only exists as the lightest mass mode of the particle on the interval $-y_1 = -1$ and 0. All subsequent modes have a positive mass, and so are not consistent with the tachyon. In the ghost regime, however all modes are consistent with the ghost because all produce a kinetic term $N^2 < 0$, so all particles with masses corresponding to a brane kinetic term sufficiently negative will produce an unphysical result.

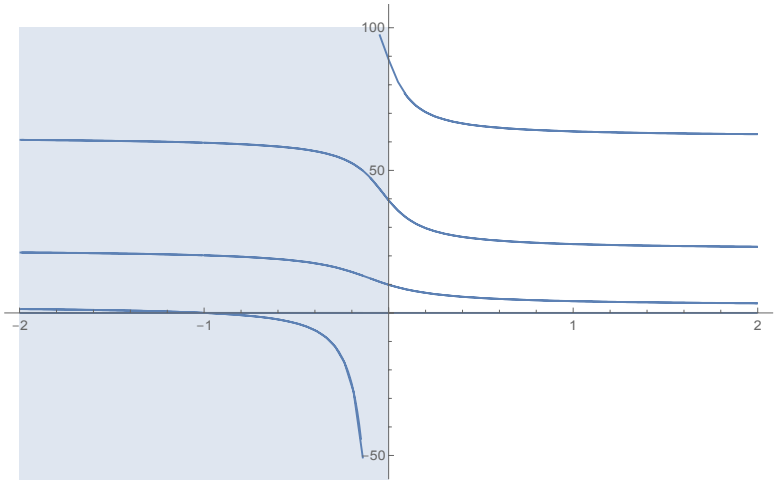

FIGURE 1. Numerical solutions for the masses of the first, second and third KK modes as a function of the brane kinetic term d_i including the massless flat solution.

For $d_1 > 0$, we find solutions with real masses and positive kinetic terms. The tachyon regime exists between $0 > d_1 > -y_1$ where the masses of the lighter modes are imaginary, and therefore tachyonic. In the darker blue shaded region, when $d_1 < -y_1$, we find the ghost regime, where the lightest non-zero mass is real but where the kinetic term becomes negative. For the numerical graph, we have taken the masses in units of $1/y_1$ (i.e., $y_1 = 1$) and we see the masses are consistent with $m^2 = n^2\pi^2 \,/\, y_1^2$ in the limit of no kinetic term ($d_1 = 0$)

Outlook

In this article we have studied the possibility of adding brane localized kinetic terms to an extradimensional theory of a scalar field. We have considered the simplest case of a flat extra dimension and moreover the bulk and brane masses for the scalar field were neglected for clarity.

We have shown how a negative brane kinetic term can have disastrous effects on the effective theory emerging from the 5D action. For small values of the negative brane kinetic term a tachyon solution emerges, showing an instability of the setup. For much larger (negative) brane kinetic terms, the tachyon solutions disappears but now a ghost appears showcasing even worse instabilities in the setup.

Although our main result is a negative result, it can still be useful for model building as it is clear that wrong sign brane kinetic terms are incompatible with a well behaved 4d effective theory, and thus should not be considered. Of course, our results must be extended to the case of non-vanishing masses for the scalar field. Also the metric background considered could have some warping, and finally we should also consider the case of fermion and tensor fields with negative brane kinetic terms. Intuitively all these situations will be problematic when negative brane kinetic terms are considered, but we leave these more involved lines of research for future studies.

Acknowledgments

We thank Dawson College and SPACE for supporting student participation in research projects. M.T. would like to thank FRQNT for partial nancial support under grant number PRCC-191578.

References

1. V. A. Rubakov and M. E. Shaposhnikov, Phys. Lett. B 125 (1983) 136.
2. K. Akama, Lect. Notes Phys. 176, 267 (1982) [arXiv:hep-th/0001113].
3. I. Antoniadis, Phys. Lett. B 246, 377 (1990).
4. J. D. Lykken, Phys. Rev. D 54, 3693 (1996) [arXiv:hep-th/9603133].
5. N. Arkani-Hamed, S. Dimopoulos and G. R. Dvali, Phys. Lett. B 429, 263 (1998) [arXiv:hep- ph/9803315].
6. I. Antoniadis, N. Arkani-Hamed, S. Dimopoulos and G. R. Dvali, Phys. Lett. B 436, 257 (1998) [arXiv:hep-ph/9804398].
7. L. Randall and R. Sundrum, Phys. Rev. Lett. 83 (1999) 3370 [arXiv:hep-ph/9905221].
8. L. Randall and R. Sundrum, Phys. Rev. Lett. 83, 4690 (1999) [arXiv:hep-th/9906064].
9. F. del Aguila, M. Perez-Victoria and J. Santiago, JHEP 0302, 051 (2003); F. del Aguila,
10. M. Perez-Victoria and J. Santiago, JHEP 0610, 056 (2006).
11. H. Davoudiasl, J. L. Hewett and T. G. Rizzo, Phys. Rev. D 68, 045002 (2003); H. Davoudiasl,
12. J. L. Hewett and T. G. Rizzo, JHEP 0308, 034 (2003).
13. M. Carena, E. Ponton, T. M. P. Tait and C. E. M. Wagner, Phys. Rev. D 67, 096006 (2003);
14. M. Carena, A. Delgado, E. Ponton, T. M. P. Tait and C. E. M. Wagner, Phys. Rev. D 71, 015010 (2005).

Differences in Anatomical Connectivity Between Cocaine Users and Healthy Controls

Arthur Ayestas Hilgert, Norman Kong, and Amanda Walsh

Abstract

In 2015, 37 million years of "healthy" life lost (DALYs) were attributed to cocaine use disorders according to the United Nations Office on Drug and Crime (2017). This study examines differences in brain connectivity between recreational cocaine users and individuals who do not use cocaine. Diffusion tensor imaging was used to study the connectivity of 45 psychotropic-medication-free individuals aged 18-40. 19 of which were healthy drug-naïve individuals, and 26 of which were recreational cocaine users. Preliminary results revealed no significant difference in anatomical connectivity between cocaine users and healthy controls. Future studies should be done using region of interest analyses.

Introduction

Approximately 371 million adults (ages 15-64) worldwide consumed drugs in 2015 (United Nations Office on Drug and Crime, 2017). Previously conducted studies suggest that those who have developed substance use disorders have prevalent changes in cortico-subcortical limbic and cognitive pathways (Goldstein & Volkow, 2011; Hyman et al, 2006; Koob & Volkow, 2010). To investigate the effects of cocaine use, we used diffusion tensor imaging (DTI) to look at differences in anatomical connectivity regarding reward pathways within cortico-limbic structures (Kober et al, 2010) between cocaine users and healthy controls.

Methods

This study was conducted using diffusion tensor imaging (DTI). This method tracks the diffusion of water molecules within various brain tissues, such as cell membranes. The examination of molecule movement allows for a non-invasive inspection of the brain on a microscopic level, which is more in-depth when compared to conventional methods like traditional imaging, constrained by millimetric image resolution. Anisotropic diffusion within the brain provides the means for a statistical analysis of structural features of neural tissues (more precisely, axons within white matter) and changes within brain connectivity (Bihan, 2006). 45 psychotropic-medication-free subjects aged 18-40 were studied. 19 of which were healthy drug-naïve individuals, and 26 of which were recreational cocaine users. Participants were scanned using a 3T Siemens Magnetom Trio MRI scanner. Twenty-five subjects had data acquired in 64 gradient directions with a b-value of 1000s/mm^2. Twenty subjects had data acquired in 60 directions, also with a b-value of 1000s/mm^2. For all participants, one reference scan was acquired with a b-value of zero. Another b-0 scan was acquired with reverse phase encoding directions to conduct topup preprocessing. The DTI data was preprocessed and analyzed with the FMRIB Software Library (FSL). Eddy current correction (Andersson et al., 2016b), using the option to replace outliers (Andersson et al., 2016a), was used to correct for signal dropout caused by patient motion and eddy currents caused by the rapid switching of the diffusion weighting gradients. Topup correction was used primarily to correct for the inhomogeneity of magnetic properties of brain tissue. Using DTIFIT in FSL, fractional anisotropy files were generated, which fits a diffusion tensor model at each voxel (Figure 1). In order to conduct a voxel-wise statistical analysis of the brain (more specifically, using the FA data) between the cocaine users and healthy controls, tract-based spatial statistics was used (TBSS) (Smith et al., 2006) (Smith et al., 2004).

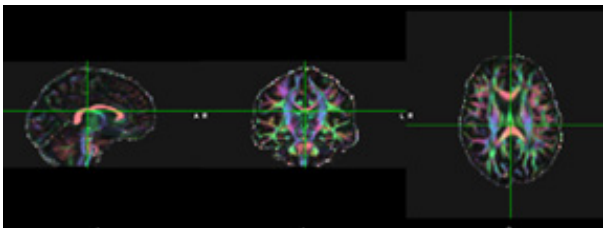

Figure 1: Fractional anisotropy map of 1 individual (FA map). Colors indicate different tract directions: blue is top to bottom, red is left to right, green is front to back.

Results

Preliminary results reveal no significant differences in anatomical connectivity between cocaine users compared to healthy controls. As illustrated in Figure 2, TBSS only demonstrated a noticeable difference in the brain tracts at a low, non-significant 1-p threshold of 0.7 (p = 0.3). At p-values below 0.3, no difference in connectivity could be observed on the FA skeleton overlay generated by TBSS. A p-value greater than 0.05 fails to reject the null hypothesis.

Conclusion

No significant difference was observed in anatomical connectivity between cocaine users and healthy controls. These results do not concur with existing research on this topic (Goldstein & Volkow, 2011; Hyman et al, 2006; Koob & Volkow, 2010). Limitations include a conservative methodological approach by using whole-brain voxel wise analysis. Future studies should be done using region of interest analyses, which may increase the accuracy of the results. In addition, different acquisition parameters were used between the 2 sets of participants which may have introduced more noise. Lastly, a small sample size of only 45 participants was collected, however the study is currently ongoing, remedying this issue.

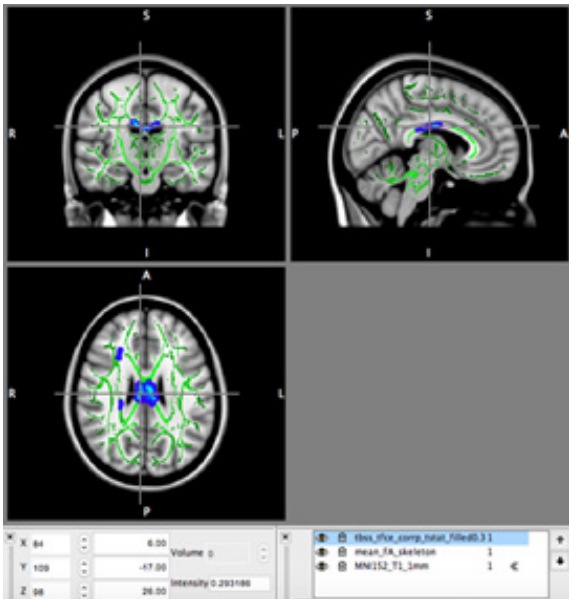

Figure 2: The threshold of TBSS results was 1-p = 0.7 (p=0.3). This contrast, in blue, was created to illustrate the increased connectivity within drug users compared to healthy controls, which was then overlaid onto a high quality standard acquired from the Montreal Neurological Institute (MNI) in order to give structural context. A mean FA skeleton, in green, was added, which is an alignment-invariant representation of the centres of all tracts common to a collection of data and indicates which standard-space voxels were used in TBSS (TBSS, 2012).

Acknowledgements

Dr. Sylvia Cox, our supervisor from the department of psychiatry at McGill University

Dr. Marco Leyton, the principal investigator of this project from the department of psychiatry at McGill University

Dr. Helene Nadeau, organizer of the internship and professor at Dawson College

Stephanie Scala and Valerie D'amour-Horvat, Ph.D. students responsible for data acquisition

References

1. Andersson, J. L., Graham, M. S., Zsoldos, E., & Sotiropoulos, S. N. (2016a). Incorporating outlier detection and replacement into a non-parametric framework for movement and distortion correction of diffusion MR images. *NeuroImage,141*, 556-572. doi:10.1016/j.neuroimage.2016.06.058
2. Andersson, J. L., & Sotiropoulos, S. N. (2016b). An integrated approach to correction for off-resonance effects and subject movement in diffusion MR imaging. *NeuroImage,125*, 1063-1078. doi:10.1016/j.neuroimage.2015.10.019
3. Bihan, D. L. (2006). Looking into the functional architecture of the brain with diffusion MRI. International Congress Series, 1290, 1-24. doi:10.1016/j.ics.2006.04.006
4. Goldstein, R. Z., & Volkow, N. D. (2011). Dysfunction of the prefrontal cortex in addiction: Neuroimaging findings and clinical implications. *Nature Reviews Neuroscience,12*(11), 652-669. doi:10.1038/nrn3119
5. Hyman, S. E., Malenka, R. C., & Nestler, E. J. (2006). NEURAL MECHANISMS OF ADDICTION: The Role of Reward-Related Learning and Memory. *Annual Review of Neuroscience,29*(1), 565-598. doi:10.1146/annurev.neuro.29.051605.113009
6. Kober, H., Mende-Siedlecki, P., Kross, E. F., Weber, J., Mischel, W., Hart, C. L., & Ochsner, K. N. (2010). Prefrontal-striatal pathway underlies cognitive regulation of craving. Proceedings of the National Academy of Sciences, 107(33), 14811-14816. doi:10.1073/pnas.1007779107
7. Koob, G.F., & Volkow, N.D. (2010). Neurocircuitry of addiction. Neuropsychopharmacology, 35, 217-238.
8. Smith, S. M., Jenkinson, M., Woolrich, M. W., Beckmann, C. F., Behrens, T. E., Johansen-Berg, H., . . . Matthews, P. M. (2004). Advances in functional and structural MR image analysis and implementation as FSL. *NeuroImage,23*. doi:10.1016/j.neuroimage.2004.07.051
9. Smith, S., Jenkinson, M., Johansen-Berg, H., Rueckert, D., Nichols, T., Mackay, C., . . . Behrens, T. (2006). Tract-based spatial statistics: Voxelwise analysis of multi-subject diffusion data. *NeuroImage,31*(4), 1487-1505. doi:10.1016/j.neuroimage.2006.02.024
10. TBSS. (2012, April 09). Retrieved May 10, 2019, from https://fsl.fmrib.ox.ac.uk/fsl/fslwiki/TBSS
11. United Nations Office on Drugs and Crime. (2017). World Drug Report 2017. *UNODC Research,* 2-2. doi:10.18356/c595e10f-en

Correlations between Cortical Thickness and Cognitive Functions in Normally Developing Children

Tudor Chira, Will Sze, Budhachandra Khundrakpam

Abstract

Cortical thickness is often linked to cognition in developing children. The goal of this research was to observe how the cortical thickness correlates with differences in cognitive functions such as vocabulary, reading, and attention. Data was taken from the Pediatric Imaging, Neurocognition and Genetics study (PING) database which consists of normally developing subjects including those with ADHD and other similar conditions, since these types of disorders are fairly common in the population. Data processing was done through CIVET, an automated pipeline, to measure cortical thickness. This was followed by a visual quality control to ensure that the cortical thickness measurements were not affected by artifacts such as motion. Using SurfStat, a toolbox for Matlab, it was noted that cognitive abilities such as the level of vocabulary and attention were not significantly related to cortical thickness by multiple comparisons correction at cluster threshold $p = 0.001$. However, higher reading skills showed significant correlations with an increased cortical thickness in the occipital lobe of the right hemisphere and in the parietal region of the left hemisphere. These findings indicate that some cognitive functions can relate to the cortical thickness while others do not or have a more subtle correlation.

Introduction

The cerebral cortex is composed of gray matter substance where about 14 billion of neurons can be found [4]. Different areas of the brain can have different cortical thickness, and different behaviours can affect this thickness. In fact, the cortical thickness is often associated with cognition and behaviours in developing children [3]. There have been many studies on the cortical thickness namely the London taxi driver study done by the Institute of Neurology at University College London, and a study comparing musicians to non-musicians done by the Montreal Neurological Institute. It has been found that London taxi drivers have thicker cortices than average people in the hippocampus and that the size increases with experience, allowing them to have greater spatial awareness[5]. In the musician study, musician subjects had thicker cortices than non-musicians in their superior temporal lobe where the auditory function is processed, as well as in their lateral frontal lobe where complex problems are solved [1].

In a similar way, the goal of this project was to analyze the change in cortical thickness within different cognitions in subjects and their interaction with age. The cognitive abilities include level of vocabulary, attention skills, and reading skills. The findings of this study could help better understand how the brain develops as a person learns and enhances their skills, and how the cortical thickness influences the cognitive abilities of developing individuals.

Methods

PING database

The data used in this project is from the Pediatric Imaging, Neurocognition, and Genetics study database [8]. The data was composed of about 1500 subjects that were recruited through different sites across the United-States: Baltimore, Honolulu, Los Angeles, New Haven, New York, Sacramento and San Diego. The subjects, only scanned in MRI machines in a single visit, were normal developing subjects from 3 to 22 years old. The exclusion criteria are history of brain disorders, brain injury, prematurity, drug and alcohol ingestion for more than three months, trauma with more than 30 minutes of loss of consciousness, etc. Participants with learning disabilities or ADHD were included since these conditions are common in the population. In order to collect participants' medical information, questionnaires were provided to the guardians of minors (18 years and under). The medical information of the participants over 18 years was self-reported.

The NIH toolbox was used to assess their cognition and behaviours. Vocabulary comprehension is tested by asking the participant to choose one of many pictures which best matches a given word. Reading recognition is assessed orally. The subject must pronounce letters and words to the best of his ability regardless of whether he understands the words or not. Finally, attention is measured using the flanker test where the direction of an arrow must be correctly evaluated in a stimulating environment. More details can be found on the NIH toolbox's website [9].

Data processing - CIVET

The data was processed through CIVET, a pipeline developed by the MNI that is able to measure the thickness, morphometry and volume of the cortex [2]. The steps include:

1) Registering the native scans to a standardized space (stereotaxic space) using the ICBM 152 template;

2) Correcting for non-uniform intensity to distinguish white matter and gray matter boundaries as well as the grey matter surface (pial);

3) Masking the brain to exclude unwanted tissues;

4) Classifying the tissue as white matter, gray matter and cerebrospinal fluid;

5) Creating a Deformable mesh at the white and gray matter boundary and at the pial surface. The distance between

these meshes can then be measured;

6) Extracting the surfaces by reducing a sphere down to the white matter surface using 81920 polygons and expanding to the gray matter surface. This allows for a 3D representation;

7) Registering the surfaces to the ICBM 152 template to be able to compare at the vertex level.

Visual Quality Control

A visual quality control was done to ensure that there is no erroneous data in our sample. This is crucial since artifacts such as motion can lead to an underestimation of the cortical thickness. This includes looking at surface extractions; intersections between the white and the pial surfaces; motion in the scans; and quality of registration, of tissue classification and of the deformable mesh. Ratings for each aspect and subject were done in a spreadsheet using the following notations: 0 as a fail, 1 as an uncertainty and 2 as a pass. Images which were badly processed or involving motion were excluded from the sample. 672 subjects were analyzed. Of these, 509 have passed the quality control. This final number was used to plot the mean cortical thickness (figure 1), but due to lack of some subjects' recorded data in the assessment, the sample is reduced to 503 subjects for the analysis of the reading cognitive task.

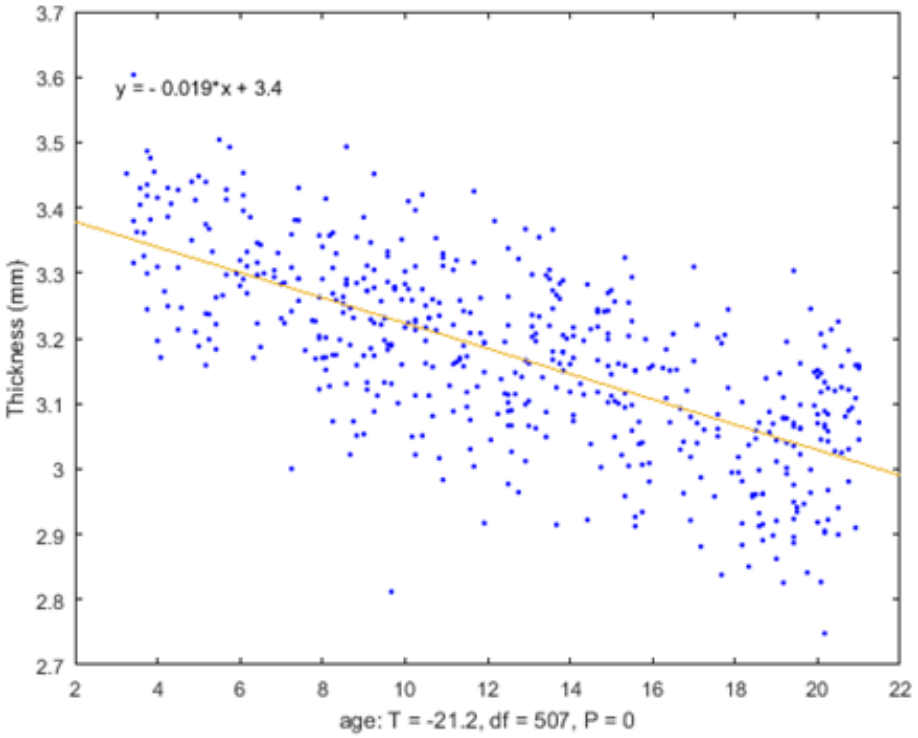

Figure 1: The mean cortical thickness with age in a sample of 503 subjects. The linear equation shows a decrease of 0.019 mm per $year$.

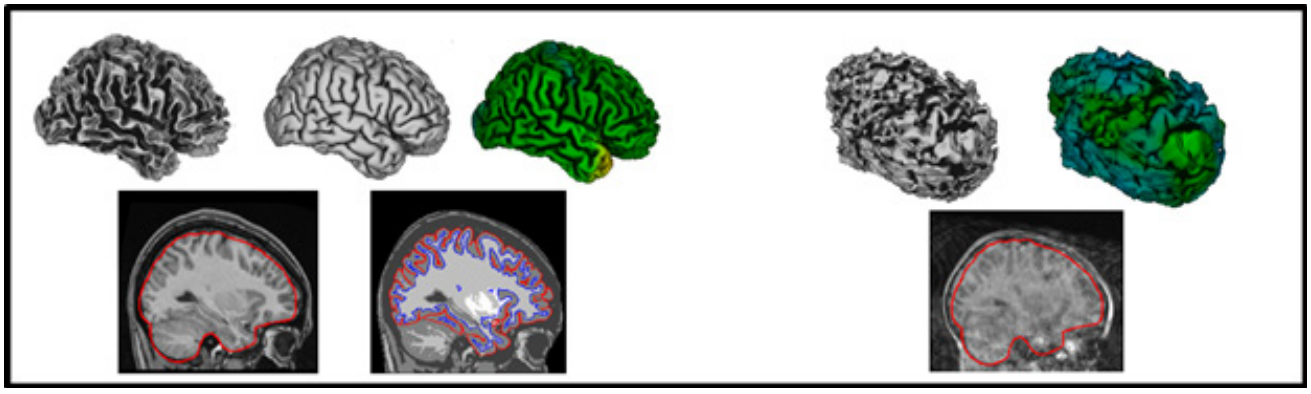

Figure 2: Difference between good surface extraction (Left) and bad surface extraction due to motion (right) in the images and data processed by CIVET.

Statistical Analysis

Statistical analysis was done using SurfStat, a toolbox for Matlab developed by Keith J. Worsley from McGill University. The median of the scores was calculated in order to assign high and low cognitive function levels to each subject. A comparison of the cortical thickness between the two levels is first done by creating a linear model and then generating t-values, P-values and Q-values on a 3D brain map. These values can be interpreted in a similar way as they would be interpreted in a typical statistical analysis. Each of the vertices that make up the polygons in a subject's image are analyzed with every other subject's respective vertices to get the t-value. For example, the 3823rd vertex of every subject will have a specific cortical thickness value and will undergo a t-test. This will output a t-value for the part of the brain that corresponds to the 3823rd vertex. The t-value maps are used to visualize the t-statistics at each vertex using a color code: the warmer the colors, the higher the t-values. A t-value above 0 means an increasing thickness whereas a negative value indicates a decreasing thickness in the particular area of the brain that is associated to that value. The P-value map shows a visualization of high t-values with random field theory corrected surviving a cluster threshold of 0.001 by default. It is the probability of obtaining a certain t-value and therefore the probability of the results being due to chance. The lower the cluster threshold, the smaller the chance for false positives is in cluster values. On a P map, the significance of clusters (groups of vertices) and single vertices can be observed separately. Finally, the Q-value map visualizes the false discovery rate set at a threshold of 0.05 by default allowing for a higher acceptance of false positives [7]. Worsley's documentation was used to code the models and maps [7].

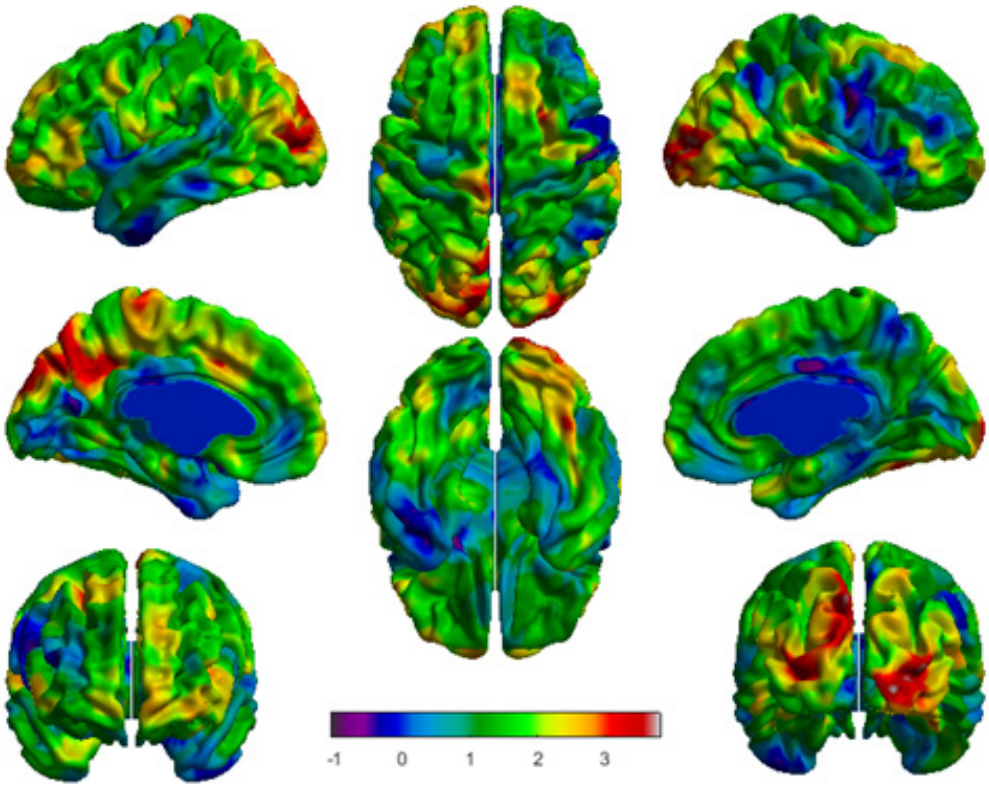

Figure 3: T map (499 df) for reading high-low medians correcting for age (n = 503). The colors show thickness difference between higher and lower levels of reading skills. Low to high difference are represented by cool to warm colors.

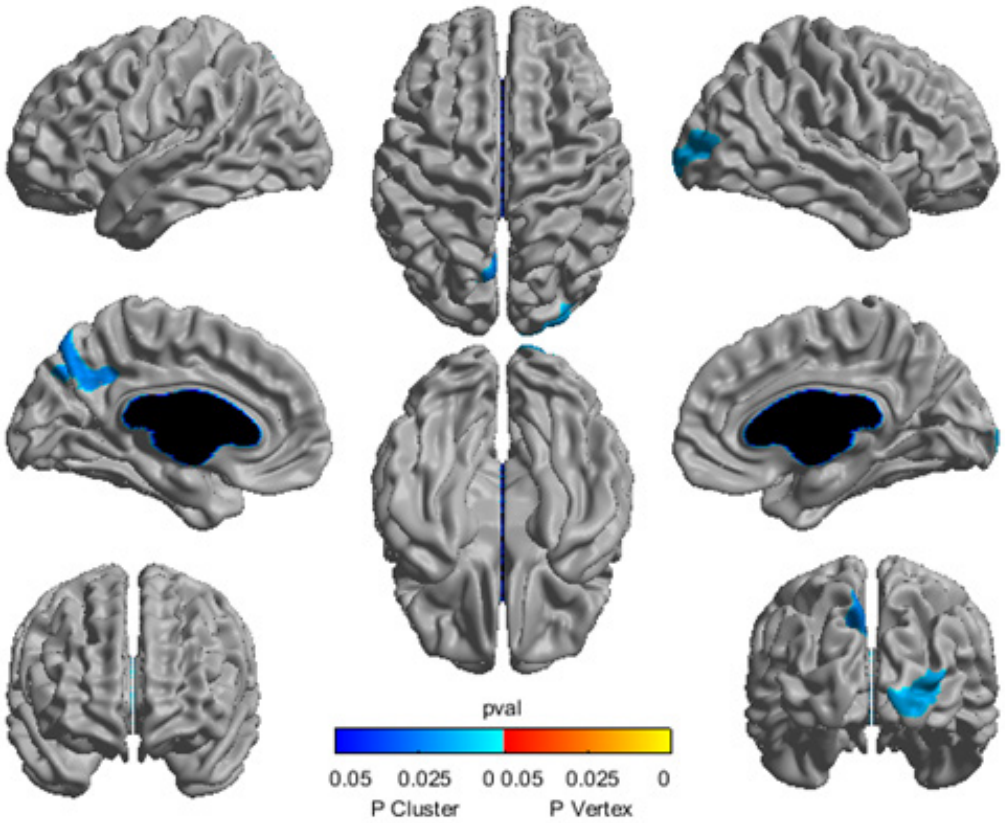

Figure 4: P-values for reading high-low medians correcting for age ($n = 503$). Significant difference at the cluster level can be found in Brodmann areas 7 and 17. No significant difference can be found at the vertex level.

Results and Discussion

Development happens at a different age in every person and affects each individual differently. In order to generate and analyze accurate brain maps outputted by Matlab, the general linear model is used and controlled for the age and gender of the subjects. The model is of the form $M = 1 + Age + Gender + (\boldsymbol{test\ variable})$ to test for the effects of the variables [7]. By looking at brain maps showcasing the t and P-values as the ones displayed in figure 2 and 3, we found no significant correlation between vocabulary results and cortical thickness after looking at various brain maps such as the interaction that reading and cortical thickness can have with age as well as gender differences. The same applies for attention results. However, it was found that the 256 subjects that scored above the median out of 503 subjects that passed quality control in reading had a higher cortical thickness in the right occipital and left frontal lobes colored in blue on the P-value map (using a strict p cluster threshold of 0.001). These areas are more specifically Brodmann areas 7 and 17 which are associated with visuo-motor coordination and the primary visual function respectively. The primary visual function allows the processing of visual information, so it is understandable that it plays a role in reading. Area 7, however, is less straightforward and leaves only room for speculation. It is important to note that Brodmann area 40 which is linked to reading does not appear to have an increased thickness for skilled readers. This can be explained by the fact that although a thicker cortical thickness is most of the time associated with higher cognitive abilities, the reverse can also be true in some cases. This has been observed in other studies such as the musician study mentioned above [1].

No other studies have been found relating cortical thickness and reading skill during development in similar age groups. However, the mean cortical thickness and its development with age were similar to previous studies in general although there were a few differences. For example, the mean cortical thickness decreased linearly with age at a rate of about $0.019\ mm\ per\ year$ between the ages of 3.75 and 22 years old (figure 3) as opposed to the Ducharme et al. study that had a decrease of $0.027\ mm\ per\ year$ between 5 and 22 years old [3]. However, this discrepancy could be explained by the different populations studied, the slight age difference and the multiple testing that was done in the Ducharme study. More importantly, this study has a smaller number of subjects from 4 to 8 years old compared to other age ranges while the Ducharme study has a more homogeneous age distribution.

Sources of errors could have been eliminated by a stricter quality control allowing only the very best images to pass. This would have ensured that only the scans with

the smoothest and thus better processed surfaces are observed. However, it would have reduced the sample size, potentially giving less accurate results. Other possible errors could come from the automatic process done by CIVET. Furthermore, although the NIH toolbox is overall very reliable, multiple testing could have ensured more solid and meaningful results for each cognitive function. In addition, development happens at a different age in every person and affects everybody differently. Even with a general linear model that corrects for age, there is still a degree of uncertainty in the data because children develop cognitive faculties at various ages. More complex linear models may give improved results. Furthermore, with a t-test for every small area of the brain, the number of false positives can be very high. This is mostly corrected by the lowered p cluster threshold, but is still worth considering as one of the principal sources of error.

Conclusion

To sum up, the cortical thickness of the right occipital and left frontal lobes or, more specifically, in the Brodmann areas 7 and 17, in subjects with above the median results in reading was found to be higher than that of those who were below the median. In addition, it appears that there is no significant correlation between cortical thickness, vocabulary and attention.

For future experiments, it would be interesting to look at how the mean cortical thickness evolves with age in the brain areas aforementioned that seem to be related to good reading skills. This could offer insight on how this particular skill is developed in the brain. It was also found that good reading skills correlate with a part of the brain that processes visual input. A subsequent study could look at how this changes with blind test subjects.

Acknowledgements

Many thanks to Dr. Hélène Nadeau and Dr. Sylvia Cox without whom we would not have had the opportunity to work on this research project. We are indebted as well to Dr. Budhachandra Khundrakpam who invited us into Alan Evans' lab, guided us throughout our project and taught us a ton of things to name a few of his contributions. We would also like to thank Claude Lepage, Christopher Steel and everybody else in the lab who welcomed us and helped us with our research. Finally, thanks to all the teachers, talkers and students from Dawson who contributed to this unique learning experience.

References

1. P. Bermudez, J. P. Lerch, A. C. Evans, and R. J. Zatorre, "Neuroanatomical Correlates of Musicianship as Revealed by Cortical Thickness and Voxel-Based Morphometry," Cerebral Cortex, vol. 19, no. 7, pp. 1583–1596, Dec. 2008.
2. McConnell, "CIVET," BIC, 13-Oct-2016. [Online]. Available: http://www.bic.mni.mcgill.ca/ServicesSoftware/CIVET. [Accessed: 14-May-2019].
3. S. Ducharme, M. D. Albaugh, T.-V. Nguyen, J. J. Hudziak, J. Mateos-Pérez, A. Labbe, A. C. Evans, and S. Karama, "Trajectories of cortical thickness maturation in normal brain development — The importance of quality control procedures," NeuroImage, vol. 125, pp. 267–279, Jan. 2016.
4. J. Lerch, "Measuring Cortical Thickness," thesis, 2001.
5. E. A. Maguire, K. Woollett, and H. J. Spiers, "London taxi drivers and bus drivers: A structural MRI and neuropsychological analysis," Hippocampus, vol. 16, no. 12, pp. 1091–1101, 2006.
6. [6] L. M. Wierenga, M. Langen, B. Oranje, and S. Durston, "Unique developmental trajectories of cortical thickness and surface area," NeuroImage, vol. 87, pp. 120–126, Feb. 2014.
7. K. J. Worsly, "A Matlab toolbox for the statistical analysis of univariate and multivariate surface and volumetric data using linear mixed effects models and random field theory," SurfStat, 26-Sep-2008. [Online]. Available: http://www.math.mcgill.ca/keith/surfstat/. [Accessed: 14-May-2019].
8. [8] Data collection and sharing for this project was funded by the Pediatric Imaging, Neurocognition and Genetics Study (PING) (National Institutes of Health Grant RC2DA029475). PING is funded by the National Institute on Drug Abuse and the Eunice Kennedy Shriver National Institute of Child Health & Human Development. PING data are disseminated by the PING Coordinating Center at the Center for Human Development, University of California, San Diego.
9. "NIH Toolbox Cognition Batteries," HealthMeasures, Available: http://www.healthmeasures.net/explore-measurement-systems/nih-toolbox/intro-to-nih-toolbox/cognition?fbclid=IwAR30SrGG7JI3TlO-6bIaMJ3qeyo66xVPMBricggPayR9RHz31gJFnJlixi6U [Accessed: 15-May-19]

Influence of Bisphenol-A (BPA) on the Egg Reproduction of Ramshorn Snails (Planorbula sp)

Ashley Spanier-Levasseur, Chaimaa Ouizzane, Dylan Stermer, Eliana Rohr,
Erica Cianfarano, Jennifer Pham, Mikaela Piccirelli and Olivia Di Domenico

Abstract

Bisphenol A (BPA) is a man-made chemical used in manufacturing plastics. This chemical frequently comes into contact with aquatic systems through chemical leakage from both the manufacturing process and wastewater runoff. BPA's estrogen-like composition gives it the ability to act as an endocrine (hormone) disruptor on reproduction of organisms living in aquatic environments. The objectives of this experiment are to understand the effects of BPA on the reproductive output of aquatic invertebrates using Ramshorn Snails, hermaphroditic organisms, as well as studying the short-term repercussions of BPA on this species during a 6-week experiment. We hypothesized that BPA would decrease reproductive output of Ramshorn snails. To test this, six pairs of snails were exposed to BPA-concentrated water and five pairs of snails were exposed to dechlorinated water and kept under controlled conditions for 6 weeks. The number of eggs were counted on a weekly basis. The results of the t-test revealed that the number of eggs laid by the BPA exposed snails was significantly larger than the number of eggs of the snails not exposed to BPA, which contradicts our hypothesis. This phenomenon can be explained by the presence of BPA which encourages the enlargement of the female sex organs, giving the snails the ability to produce more eggs that could possibly be fertilized by the sperm from the male sex organs, despite the fact that the sperm production count is lower. Moreover, due to the short nature of the experiment, no possible long-term effects of BPA exposure on the health of the organism had arisen.

Introduction

Bisphenol A (BPA), is a high production volume chemical used in manufacturing polycarbonate plastics and epoxy resins in nearly every industry and can be found in many household products such as canned goods and plastic containers (Mileva et al., 2014). BPA finds its way into various aquatic environments through different forms of pollution such as emission from plastic manufacturing plants, plastic deterioration in the environment and wastewater treatment plant discharge (Corrales et al., 2015). BPA is also an endocrine disruptor which means it affects hormone levels by mimicking or irritating hormones that occur naturally in the body (Damstra et al. 2002), specifically that of estrogen, which regulates reproduction. This is problematic because BPA mimics the hormone estrogen and thus can cause overstimulation (NIEHS 2015). Given that BPA is capable of disrupting reproduction, its presence in the environment can affect the organisms present. BPA is water-soluble (Staples et al. 1998) which will greatly affect many aquatic species by its introduction to aquatic ecosystems through liquid waste from landfills and through the disposal of BPA based products into water (Staples et al. 1998).

Invertebrates make up around 95% of all animals (Canesi & Fabbri 2015) and therefore play an essential role in most ecosystems. The Ramshorn snail, for example, is an important part of the aquatic ecosystem based on their ecological role in the aquatic food web and their ability to maintain a biologically sustainable water quality. Certain chemicals can interfere with normal function of the reproductive system of Ramshorn snails, among them is BPA which is particularly interesting due to its relative abundance and high concentrations in the environment (Huang et al. 2011).

Our current understanding of the effects of BPA exposure is limited. However, the discoveries made in the field tend to suggest that BPA is harmful. Other than interfering with hormone levels, BPA has been shown to induce super-feminization in Ramshorn snails (Oehlmann et al. 2006). This means that female sex organs become enlarged and male sex organs decrease in size.

Past studies conducted on the presence of BPA concerning invertebrates have revealed that the research is incomplete and often fragmented due to a large number of species with great diversity (Canesi & Fabbri 2015). It is important to understand the effects that BPA has on all species, including invertebrates, in order to protect complete ecosystems and avoid the extinction of certain species.

Our project aims to improve our understanding of the effects of BPA exposure on fertility rates of Ramshorn snails by examining how the presence of BPA affects the reproductive output of these snails. We exposed snails to BPA for six weeks, recorded the number of eggs and compared it to snails that were not exposed to BPA. Given that BPA is a known endocrine disruptor shown to cause "super-feminization" in snails, we hypothesized that the snails exposed to the BPA solution would have a lower output of eggs than the snails not exposed to BPA due to an unequal production of gametes (lower sperm count) destabilizing normal fertilization.

Materials and Methods

Ramshorn snails were ordered from the Ward's Science website Wardsci.com. Once the snails arrived at Dawson College (Montreal, QC, Canada), there was a ten-day acclimatization period where they were kept in a BPA free tank filled with dechlorinated water. During these initial ten

days, the snails were given 3 pieces of chalk (about 1 cm) and fed lettuce as necessary.

Five containers (BPA-free plastic, 500mL, hole punched covers) were filled with 300mL of dechlorinated water, and six identical containers were filled with 300mL of the 60 µg/L BPA solution made by diluting a 2.0 mg/L BPA stock solution (SIgma-Aldrich ≥99%) with dechlorinated water. Two snails were placed in each container for a total of 22 snails. A piece of chalk approximately 0.3 x 0.5 cm in size was placed in each container as a source of calcium carbonate with an approximately 4 x 5 cm piece of hydroponic Boston lettuce, washed twice with distilled water, as food. A new piece of lettuce was added to the container once a week, whereas the chalk, dechlorinated water, and BPA solution were replaced every two weeks after the entirety of the containers were removed. All containers were kept in the same windowless room at room temperature. The snails were only exposed to a lamp timed precisely for eight hours of light and sixteen hours of dark.

Twice a week, for six weeks, all new egg masses found on the sides of the containers (not floating) were circled and marked with the week they were counted. A magnifying apparatus was used to count the number of eggs in the egg masses that were produced. After the sixth week, the shell size of each snail was measured and recorded. One-tailed t-tests were performed (website: http://www.socscistatistics.com/tests/ttestdependent/Default2.aspx) with a significance level of 0.05 to determine if there were statistically significant differences between the average amount of eggs produced by the control and experimental group. Only the average number of eggs of weeks three to six were inputted into the tests. Weeks one and two were not included within the analysis. A t-test was also performed to ensure there were no differences between snail shell sizes.

Results

The amount of eggs produced by ramshorn snails not exposed to BPA was significantly greater than that of the snails exposed to BPA (p=.006737). Snails exposed to BPA (n=6), laid an average of 119 eggs total for the average of weeks 3-6. For snails not exposed to BPA (n=5), the average number of eggs laid was of 58 eggs for the same time period (Figure 1).

Additionally, statistical analysis of the snails' shell size indicated no significant difference between the shell size of snails exposed to BPA (diameter mean = 14.75 mm) and snails not exposed to BPA (diameter mean = 14.75 mm) (p=0.234) (Figure 2).

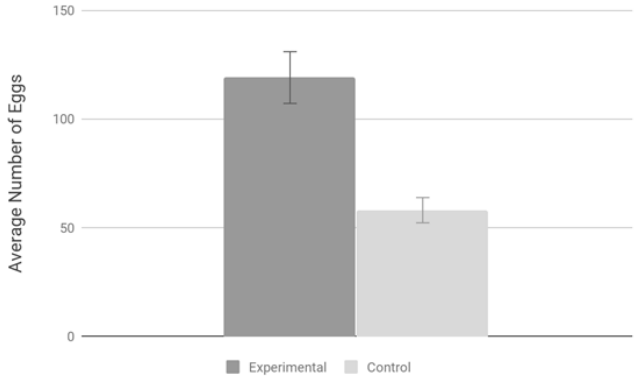

Figure 1: Mean number of eggs of weeks 3-6 produced, (n=5 for control, n=6 for experimental). Error bars represent standard deviation.Data obtained was statistically significant according to the t-test ($p < 0.05$).

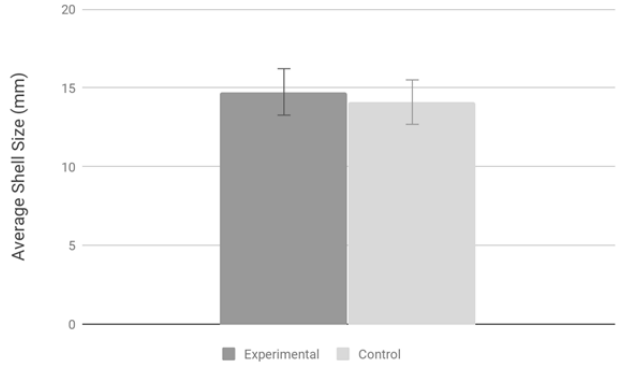

Figure 2: Mean snail shell size (mm), (n=5 for control, n=6 for experimental). Error bars represent standard deviation. Data obtained was not statistically significant according to the t-test ($p> 0.05$).

Discussion

The results of the experiment were contrary to our original hypothesis that BPA hinders the reproductive output of Ramshorn snails. In fact, the control snails produced significantly less eggs compared to the BPA exposed snails.

The reproductive success of a species depends heavily on both the health and development of the sperm and ovum producers. The sexual development of the snail is directly correlated to, and thus affected, by its living environment. Through exposure to BPA, the sexual development of the snails is altered making super females (ie. having larger female sexual organs and producing more eggs) (Oehlmann et al. 2006) and weaker males (i.e. reduced sperm count) (Jeong-Hun Kang et al. 2007). Regardless of this effect, the data shows that BPA does not reduce the amount of eggs produced by Ramshorn snails in the time period observed. Seeing as the size of a snail's shell has an effect on the amount of eggs it produces (larger snail lays more eggs), it was necessary to consider it (Anderson, Guralnik, and Weaver 2007; Bronson and Norton 2005). The average shell size difference between the experimental and control treatments was determined to be statistically insignificant. Therefore, the shell sizes of the replicates in this study have no influence on the results.

Freshwater snails lay their eggs about 14 days after fertilization (Baker et al.,1945). Since all snails were kept in one container prior to the beginning of the experiment, it is likely that they would fertilize during this period. Therefore, eggs laid during the first two weeks of the experiment were most likely fertilized before the exposure to BPA. The first two weeks were a also a time of change for the snails, as they were being moved around and needed time to settle in their new environment. Changes in temperature and water levels can cause fluctuations in freshwater snails' population (McCullough FS, 1992). Consequently, the amount of eggs produced could have been affected. By taking the data starting from week 3, we tried to ensure that the amount of eggs produced was only affected by the influence of BPA.

The results of the experiment support the research of Duft et al. (2003) on the Potamopyrgus antipodarum, an ovoviviparous parthenogenetic freshwater mud snail from New Zealand. This research showed that BPA exposed mud snails had a greater number of eggs in their brood pouch than their unexposed counterparts. Additionally, the results show that the snails exposed to BPA produced a greater amount of eggs which agrees with a study by Andersen et al. (1999) that observed that there is an increase in the egg output of the marine species Acartia Tonsa at a BPA exposure level of 20 ug/L. Furthermore, the observation that BPA as an endocrine disruptor does not negatively affect the reproductive success of the snail supports a conclusion by Oehlmann et al. (2006). All these studies suggest that the final data in this experiment falls in line with what other researchers have observed in nature.

The expected result was that BPA, being an endocrine disruptor, would reduce the egg production of the Ramshorn snail. However, with the opposite effect happening, a hypothesis can be made that endocrine disruptors do not negatively affect the reproductive output of a species over a short period of time. A method to test this hypothesis would be to replicate this experiment using other compounds known to interfere with endocrine function. If none of the endocrine disruptors involved cause a significant decrease in reproductive output, then the alternate hypothesis can be supported. Another experiment that could help investigate the effect of endocrine disruptors on reproductive output would be to perform the same experiment with several different species of snails and different organisms entirely. Similar outputs between multiple species or organisms to our results could suggest that endocrine disruptors do not negatively affect reproductive output. It would also be important to make sure that further experimentation include non-hermaphroditic animals considering they only represent a small fraction of all animal species. An experiment can be conducted where the two genders of a species are exposed to BPA environments independently and then are brought together for breading. This would effectively test how an endocrine disruptor influences the reproductive success of different genders.

In addition to changing the type of organism used, this new hypothesis can also be tested by increasing the time period of the experiment. Since we performed the experiment for a duration of 6 weeks, we were able to look more closely at the short-term effects of BPA on Ramshorn Snails. As mentioned in our original hypothesis, the number of eggs laid by the snails exposed to BPA was expected to be lower than the number of eggs laid by the snails that were not exposed to BPA. Looking at our data, that was not the case. However, all previous information we stated about the effects of BPA on the reproductive outcome of Ramshorn snails only relate to its long-term effects as an endocrine disruptor. Being a hormone disruptor does not necessarily mean the impact will be seen right away, thus the chemical might need some time to affect the non-controlled variable (number of eggs laid). The 6-week period we used to experiment might not have been enough for us to see the effect or full potential of the BPA's impact. A longer experiment could have unveiled different results as well as the chance to look at other factors affected by BPA such as egg viability. Performing this experiment short-term instead of long-term might have been a reason as to why our results do not support the original hypothesis. Moreover, in the Oehlmann study (2006), an increase in the number of eggs laid by the BPA snails was seen during the first few weeks but tremendously decreased after. If we follow Oehlmann's (2006) data pattern, since the experiment was only performed for a short period of time, it was impossible to notice the eventual decrease in the number of eggs laid.

An increase in the reproductive output of Ramshorn snails has both positive and negative consequences. For instance, in a given habitat, a large increase in egg production can lead to population growth, as long as they survive. Given a snail's major role in aquatic environment is to regulate algae growth and water quality, if a habitat is being polluted, the increased population can help maintain its health. Furthermore, snails constitute a food source for many aquatic animals, such as certain species of fish, turtles, and ducks (Johnson, 2009). Thus, these species can continue to survive and reproduce, which preserves entire ecosystems. On the other hand, population growth causes a decrease in resource availability, which can affect the balance of life in a specific habitat. With an increased fertility of Ramshorn snails, the metabolic cost of reproduction, discussed by Bronson and Norton (2005), should be considered. There is only a certain amount of energy available to one organism at a given time. If BPA causes an increase in reproduction, then more energy is being used for that one process, reducing available energy for other metabolic processes such as growth, digestion and food acquisition. This imbalance in metabolic activity can affect an organism's ability to

function and develop properly.

With continued use of plastics globally, the chances of chemicals like BPA entering aquatic environments are increasing. It is important to know what products use these chemicals in their manufacturing and if there exist alternatives to these products that are safer for the environment. Although the data collected did not suggest any negative consequences of BPA on reproductive outputs, as determined by an increase in egg production, it is still entering aquatic habitats and the effects of BPA on other organisms are uncertain. Global recognition of the potential risk that chemical pollution poses is essential for the conservation of the delicate environments that we have on earth. Canada has already banned the use of BPA plastics. However, in other countries around the world, the use of BPA is increasing each year, potentially polluting environments globally. It is the responsibility of scientists internationally to find a "natural substitute" to BPA that will have less of an effect on the biosphere.

References

1. Andersen HR, Halling-Sørensen B, Kusk KO.1999. A parameter for detecting estrogenic exposure in the copepod Acartia tonsa. Ecotoxicol Environ Saf.;44:56–61.
2. Anderson, T.K., Guralnick, R.P., Weaver, K.F.. 2007. Variation in adult shell morphology and life-history traits in the land snail Oreohelix cooperi in relation to biotic and abiotic factors. Journal of Molluscan Studies, vol.73, no.2, p.129-137; https://doi.org/10.1093/mollus/eym006
3. Baker, F. C., & Van C. H. J. 1945. The molluscan family Planorbidae, Champaign-Urbana, University of Illinois Press.
4. Bronson, Jennifer M. and Norton, Cynthia G. 2005. The Relationship of Body Size and Growth to Egg Production in the Hermaphroditic Freshwater Snail, Helisoma Trivolvis. Journal of Molluscan Studies, vol.72, no.2, p.143-147; https://doi.org/10.1093/mollus/eyi057
5. Canesi, Laura and Fabbri, Elena., 2015, Environmental Effects of BPA. Dose-Response, vol. 13, no. 3, p. 1-14., doi:10.1177/1559325815598304.
6. Corrales, Jone, et al. 2015. Global Assesment of Bisphenol A in the Environment. Dose-Response, vol. 13, no. 3, 2015, pp. 1–29., doi:10.1177/1559325815598308. Accessed on: Mar 12,2018
7. Damstra, T., Barlow, S., Bergman, A., Kavlock, R., and Van der Kraak, G. (2002). Global Assessment of the State-of-the-Science of Endocrine Disruptors. WHO publication no. WHO/PCS/EDC/02.2. World Health Organization, Geneva, Switzerland.
8. Duft M, Schulte-Oehlmann U, Weltje L, Tillmann M, Oehlmann J. 2003. Stimulated embryo production as a parameter of estrogenic exposure via sediments in the freshwater mud-snail Potamopyrgus antipodarum. Department of Ecotoxicology, International Graduate School, Aquat Toxicol. 64:437–449
9. Huang YQ, Wong CKC, Zheng JS, Bouwman H, Barra R, Wahlström B, Neretin L, Wong MH. 2011. Bisphenol A (BPA) in China: A review of sources, environmental levels, and potential human health impacts. Environmental International
10. Jeong-Hun Kang, Asai D, Katayama Y. 2007. Critical Reviews in Toxicology, 37: 607-625
11. McCullough FS. 1992. The role of molluscicides in schistosomiasis control. Geneva, World Health Organization, Geneva 27, Switzerland.12: 11-13
12. Mileva, Guergana, et al. 2014. Bisphenol-A: Epigenetic Reprogramming and Effects on Reproduction and Behavior. International Journal of Environmental Research and Public Health, vol. 11, no. 7, p. 7537–7561., doi:10.3390/ijerph110707537.
13. National Institute of Environmental Health Sciences: Endocrine Disruptors. March 2015; URL: https://www.niehs.nih.gov/health/topics/agents/endocrine/index.cfm
14. Accessed on: March 2, 2018
15. Oehlmann, Jörg, et al. 2006. Bisphenol A Induces Super Feminization in the Ramshorn Snail (Gastropoda: Prosobranchia) at Environmentally Relevant Concentrations.Environmental Health Perspectives, vol. 114, no. S-1, pp. 127–133., doi:10.1289/ehp.8065.
16. Staples DA, Dome PB, Klecka GM, Oblock ST, Harris LR. 1998. A review of the environmental fate, effects, and exposures of bisphenol A. Chemosphere 10:2149-2173

La Détection du Quorum
Une Voie vers une Thérapeutique Anti-Infectieuse Non Antibiotique

Cassandra Koukoulomatis

Introduction

Depuis la découverte de la pénicilline par Alexander Fleming en 1928, les antibiotiques furent beaucoup développés et retravaillés. Cependant, depuis leur découverte, l'utilisation des antibiotiques est devenue abusive. Par exemple, ils sont aujourd'hui utilizes de façon excessive dans l'élevage intensif des animaux, dans le traitement des virus et dans le savon. Compte tenu de la grande capacité des bactéries à s'adapter à leur environnement et à évoluer par la sélection naturelle, cet usage excessif a pour effet de créer chez les microorganismes une résistance aux antibiotiques. Cela suscite une demande pour le développement des antibiotiques plus forts pour combattre les infections et les maladies, menant ainsi à ce qu'on appelle la « crise des antibiotiques ». Cette crise crée un intérêt pour la recherche d'alternatives thérapeutiques, une d'elles étant l'inhibition de la détection du quorum. À travers son fonctionnement, la détection du quorum est utile dans la bioactivité de diverses espèces bactériennes, dont Pseudomonas aeruginosa, et présente un potentiel prometteur dans le traitement d'infections.

La détection du quorum

1.1 Description

La détection du quorum, ou, plus communément, le quorum sensing, est un système de communication entre les bactéries. Elle peut être perçue comme le « langage » des bactéries. Les bactéries communiquent en relâchant des molécules appelées des « auto-inducteurs », qui diffusent par la suite à travers leur membrane cellulaire et entrent dans le milieu. Une fois relâchés, les auto-inducteurs agissent comme des signaux entre les bactéries de même espèce et d'espèces différentes [1]. Ces inducteurs servent donc comme « mots » dans le langage bactérien. Dans un même environnement, la population bactérienne augmente jusqu'à l'atteinte d'un seuil critique. Lorsque le nombre de bactéries dans un milieu augmente, la concentration des molécules qu'elles produisent augmente de façon proportionnelle. Quand la concentration des auto-inducteurs atteint le seuil critique, les bactéries reçoivent un signal et active la transcription d'un gène. À travers la transcription, un trait génétique peut être exprimé. D'ailleurs, le mot « quorum » est un mot latin désignant « le nombre ou le pourcentage minimum de membres présents ou représentés dans une assemblée pour qu'une élection, une délibération ou une décision soit valide»[2]. Ce mot latin est donc directement lié au mécanisme fondamental de la détection du quorum, puisqu'il dépend du nombre de bactéries présentes dans le milieu. Le quorum est donc le nombre minimum de bactéries nécessaires à l'expression d'un gène. Ainsi, comme son nom l'indique, la détection du quorum est le processus à travers lequel les bactéries détectent la concentration minimum d'une molécule nécessaire à l'expression d'un trait génétique.

1.2 La découverte

La découverte de la détection du quorum date d'une étude menée avec la bactérie Vibrio fischeri (V. fischeri) dans les années 1970. V. fischeri est une bactérie marine bioluminescente, c'est-à-dire une bactérie émettant de la lumière au moyen d'une réaction biochimique [3]. Cet organisme peut vivre à l'état libre dans la mer ou en symbiose dans des organes de poissons ou de céphalopodes [4], l'exemple le plus connu étant le calmar Euprymna scolopes [7]. Lorsque deux organismes vivent en symbiose, les deux bénéficient de la relation. Dans le cas de V. fischeri vivant dans le calmar, la bactérie se nourrit des nutriments ingérés par son hôte. Le calmar, quant à lui, profite de la lumière émise par la bactérie pour se camoufler pendant la nuit; la lumière produite par les bactéries imite la lumière de la lune, éliminant ainsi l'ombre du calmar. Celui-ci peut donc se camoufler des prédateurs et des proies [6].

Lors des études faites sur V. fischeri, les chercheurs ont découvert que lorsque cette bactérie vit dans l'organe d'un animal marin, elle émet de la lumière, mais que lorsqu'elle se trouve à l'état libre, elle n'en émet aucune. À la suite de ces recherches, les chercheurs ont pu conclure que ce phénomène peut être expliqué par la détection du quorum. En effet, lorsque la population bactérienne de V. fischeri augmente dans l'organe d'un animal, la concentration d'une molécule dans la famille des homosérines lactones acylés (HLA), un auto-inducteur, finit par atteindre le seuil critique et permet aux bactéries d'émettre de la lumière [7]. Par contre, lorsque la bactérie est à l'état libre, la population bactérienne ne peut pas atteindre la densité cellulaire nécessaire pour que la concentration d'HLA atteigne le seuil critique.

Le mécanisme de bioluminescence de V. fischeri (Annexe I) est constituée des gènes luxI, codant pour l'enzyme LuxI, et luxR, codant pour la protéine LuxR. L'enzyme LuxI synthétise l'HLA, qui, lorsque présente en faible concentration, par exemple quand V. fischeri circule librement dans l'eau, ne permet aucune émission de lumière. Par contre, lorsque sa concentration atteint le seuil critique, par exemple lorsque la bactérie est présente dans l'organe d'un animal, l'HLA présente dans le milieu intercellulaire se lie à un récepteur présent sur la membrane bactérienne et la traverse. Ensuite, cet auto-inducteur se fixe à la protéine LuxR, créant un activateur transcriptionnel. Cet activateur transcriptionnel permet à l'ARN polymérase de débuter la

transcription du gène codant pour la bioluminescence et la synthétisation de LuxI [7]. Toutes les bactéries présentes dans le milieu reçoivent donc simultanément le signal d'émettre de la lumière lorsque la concentration d'HLA atteint le quorum.

Des études sur Pseudomonas aeruginosa

2.1 La description

Pseudonomas aeruginosa, car cette bactérie peut infecter une variété d'espèces, tant chez les plantes, les nématodes, les insectes, les amibes et les mammifères. Chez l'humain, une infection de P. aeruginosa présente diverses pathologies, particulièrement chez des individus ayant des défenses immunitaires diminuées (diabète, cancer, sida, etc.), causant surtout de graves pneumonies ainsi que des lésions tissulaires [7]. Cette espèce suscite aussi beaucoup d'intérêt, car elle présente un forte capacité d'adaptation à son environnement, ce qui la rend rapidement résistante aux traitements antibactériens. Sa capacité à évoluer rapidement rend les infections de P. aeruginosa difficiles à traiter, causant ainsi un taux de mortalité élevé, variant de 26 à 76% [7].

2.2 Les facteurs de virulence régulés par la détection du quorum

P. aeruginosa présente plusieurs facteurs de virulence : des molécules contribuant au pouvoir pathogène de la bactérie, la rendant capable d'infecter l'hôte et causer des symptômes. Parmi ces facteurs de virulence figurent l'élastase, la pyocyanine, l'exotonine A et les rhamnolipides, qui sont tous des facteurs régulés par la détection du quorum [7].

L'élastase est une enzyme qui hydrolyse l'élastine. L'élastine est une des protéines situées dans la matrice extracellulaire qui compose le tissu conjonctif d'un animal. P. aeruginosa a la capacité de produire de l'élastase afin de pénétrer dans la membrane cellulaire de l'hôte, augmentant ainsi sa pathogénicité [7].

La pyocyanine peut diffuser à travers la membrane cellulaire de l'hôte et causer l'apoptose des neutrophiles : des cellules immunitaires responsables de la destruction de pathogènes. Elle diminue aussi la fréquence des battements ciliaires des cils vibratils [8], des cils mobiles recouverts de mucus se trouvant dans la cavité nasale. Ces cils vibratils agissent normalement en tant que « filtres », recueillant les microbes et les poussières et les rejetant ensuite par les narines à l'aide de battements ciliaires. La pyocyanine agit donc sur deux mécanismes immunitaires, rendant l'hôte plus susceptible à l'infection.

L'exotonine A est une protéine toxique sécrétée par la bactérie, qui inhibe la synthèse de protéines dans les cellules de l'hôte [7].

Les rhamnolipides ont comme effet d'empêcher la phagocytose [10], un mécanisme immunitaire dans lequel des macrophages, des neutrophiles ou des granulocytes ingèrent ou engloutissent des pathogènes [10]. Les rhamnolipides nuisent donc à la capacité de l'hôte d'éliminer les bactéries et d'autres pathogènes.

2.3 Les trois systèmes de détection du quorum

Trois systèmes de détection du quorum ont été découverts chez P. aeruginosa (Annexe II).

Le premier système est le système las : les gènes lasI et LasR, codant pour les molécules LasI et LasR, respectivement. LasI est une molécule synthétisant la N-(3-oxododécanoyl)-L-homosérine lactone (3-oxo-C12-HSL, représentée par « C12 » dans l'Annexe II), qui est une HLA. Lorsque la concentration de 3-oxo-C12-HSL atteint le seuil critique, elle se lie à deux protéines LasR [11], créant un complexe agissant comme activateur transcriptionnel. Ce système régule l'expression de l'élastase LasB [7].

Le deuxième système de détection du quorum présent dans P. aeruginosa est le système rhl, régulant la synthèse de rhamnolipides. Dans ce système, RhlI code pour un enzyme partiellement responsable de la production de N-butyrylhomosérine lactone (C4-HSL, représentée par « C4 » dans l'Annexe II) : un auto-inducteur. Après l'atteinte de son seuil critique de concentration, la C4-HSL se lie à deux protéines RhlR. Cela forme un complexe qui active la transcription de plusieurs gènes, dont lasA, lasB, aprA et rhlI, qui sont responsables de la production de rhamnolipides [11].

Entre ces deux systèmes, il existe des interactions; le système las régule positivement le système rhl. Une régulation positive catalyse ou accélère la production d'une certaine molécule. Une régulation négative est le contraire d'une régulation positive, donc elle influence la production d'une molécule de façon négative en la diminuant ou en l'inhibant complètement.

Le potentiel en tant que thérapeutique anti-infectieuse

L'inhibition de la détection du quorum présente une possibilité de traitement d'infection non bactéricide, car au lieu de tuer la bactérie pathogène, elle atténuerait sa virulence [12]. Les systèmes interreliés de la détection du quorum produisent les molécules nécessaires à la virulence de la bactérie. En attaquant les systèmes de détection du quorum, on dégraderait la virulence et la capacité des bactéries de se répandre. Puisque les systèmes sont interreliés, on n'aurait qu'à cibler un des systèmes pour détruire tout le réseau de communication établi entre la communauté bactérienne, sa virulence.

En limitant l'expansion de la population bactérienne, ces thérapeutiques pourraient combler le problème de résistance aux antibiotiques en permettant la prescription de doses plus faibles pour le traitement d'infections. Cela diminuerait le besoin de développer des antibiotiques plus forts et pourrait même restaurer la sensibilité de certaines bactéries aux antibiotiques [22].

Conclusion

En conclusion, la détection du quorum est un système de communication entre les bactéries découvertes lors de l'étude de la bactérie marine bioluminescente, Vibrio fischeri. Dans plusieurs études faites sur des bactéries comme Pseudomonas aeruginosa, les chercheurs ont découvert qu'une grande variété de systèmes de détection du quorum interreliés existe parmi les bactéries. Une possibilité de traitement d'infections bactériennes serait d'attaquer les mécanismes de ces systèmes, créant ainsi des thérapies qui pourraient contrer le problème de résistance aux antibiotiques. Le développement de médicaments inhibant la détection du quorum représente-t-il le futur des compagnies pharmaceutiques?

Références

1. Le Berre, R. et al. « Quorum sensing : une nouvelle cible thérapeutique pour Pseudonomas aeruginosa? », Médecine et maladies infectieuses, vol. 36, no. 7, p. 350.
2. Tourev, Pierre. « Définition: Quorum », La Toupie, http://www.toupie.org/Dictionnaire/Quorum.htm, consulté le 14 novembre 2017.
3. « Bioluminescence », Futura Santé, [En ligne], [http://www.futura-sciences.com/sante/definitions/biologie-bioluminescence-6338/], (consulté le 15 novembre 2017).
4. Branger, Alain et al. Micobiochimie et alimentation (2017), Editions : Éducagri, [En ligne], [https://books.google.ca/books?id=tvxQg3cEJyoC&pg=PA39&lpg=PA39&dq=vibrio+fischeri&source=bl&ots=WCKzQh-go_A&sig=mTP9J5NiH6sESmnYB6rwg3nzNzQ&hl=fr&sa=X&ved=0ahUKEwi57ImOpMHXAhWDTCYKHaVQDKwQ6AEIUjAL#v=onepage&q=vibrio%20fischeri&f=false], (consulté le 15 novembre 2017).
5. Le Berre, R. et al. « Quorum sensing : une nouvelle cible thérapeutique pour Pseudonomas aeruginosa? », Médecine et maladies infectieuses, vol. 36, no. 7, p. 350.
6. « La bactérie qui illumine la seiche, contrôle son rythme circadien », GuruMeditation, [En ligne], [http://www.gurumed.org/2013/04/03/la-bactrie-qui-illumine-la-seiche-contrle-son-rythme-circadien/], (consulté le 14 novembre 2017).
7. Le Berre, R. et al. « Quorum sensing : une nouvelle cible thérapeutique pour Pseudonomas aeruginosa? », Médecine et maladies infectieuses, vol. 36, no. 7, p. 350.
8. Idem, p. 352.
9. Idem, p. 353.
10. Ibidem.
11. Idem 351.
12. Kipnis, É. et al. « Les thérapeutiques anti-infectieuses non antibiotiques », Réanimation, vol. 21, no. 3, pp. 303-316.

Annexe I

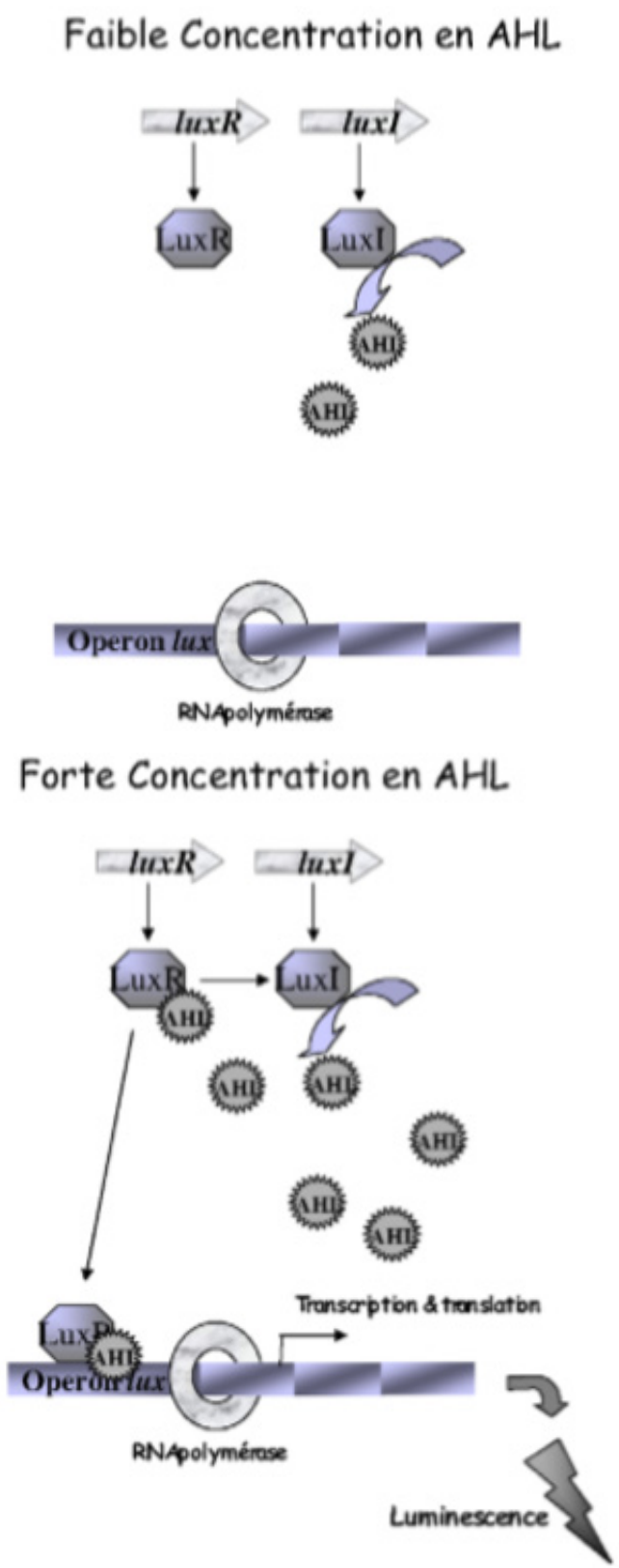

Figure 1: Schéma du mécanisme de bioluminescence de Vibrio fischeri

Courtesy of Le Berre, R. et al. « Quorum sensing : une nouvelle cible thérapeutique pour Pseudonomas aeruginosa? », Médecine et maladies infectieuses, vol. 36, no. 7, p. 351.

Solutions of an Isobaric, Inviscid Flow in Two Spatial Dimension

Jonah Saks, David Kalichman and Alexander Hariton **s**

Abstract

The goal of this paper is to solve a first-order partial differential equation using the method of characteristic strips generalized to n independent variables. The paper begins with an explanation of the method of characteristic strips. Next, it will be generalized to n variables and used to solve a partial differential equation. Finally, the solutions will be presented.

Introduction

A differential equation is an equation that relates a function to one or more of its derivatives. For example: $y' - y + 1 = 0$ where y' denotes the derivative of y with respect to some variable x. A solution of a differential equation is a function $y = f(x)$ which satisfies this equation. In the above example, one possible solution is $y = e^{x+c} + 1$, where c is some constant.

A partial differential equation (PDE) is an equation that relates a function of two or more variables to one or more of its partial derivatives, for example: $u_t + u_x = 0$.
Here, u_* denotes partial differentiation of the function u with respect to the variable *. A solution of the PDE is a function u, depending on the variables t and x, which satisfies this equation. For the example given above, one possible solution is

$u(t, x) = 2t - 2x$, since $u_t = \frac{\partial u}{\partial t} = 2$, and $u_x = \frac{\partial u}{\partial x} = -2$,

therefore $ut + ux = 2 - 2 = 0$.

Several methods exist for solving PDE's. One such method is the method of characteristic strips [1], which can be used when the PDE describes a function of two variables, though it can be generalized to n variables.

The Method of Characteristic Strips

For a given partial differential equation:

$F(x, y, u, u_x, u_y) = 0$ (1)

a solution $u(x, y)$ exists as a surface in $\{x, y, u\}$ space, called an integral surface. At any point on the surface, the vector $\vec{n}$ perpendicular to the surface is:

$$\vec{n} = \nabla\left(u\left(x,y\right) - u\right) = \left(\frac{\partial u}{\partial x}, \frac{\partial u}{\partial y}, -1\right)$$

The vector $\vec{n}$ is also the normal vector to the tangent plane at the given point. Let us denote the partial derivatives of u with respect to x and y by:

$u_x = p \qquad u_y = q$

For a fixed point on the integral surface (x_0, y_0, u_0), equation (1) becomes the equation $F(x_0, y_0, u_0, p, q)$ relating p and q, and so we can write p and q as functions of a single parameter λ:

$p = p(\lambda) \qquad q = q(\lambda)$

Since each normal vector $\vec{n}$ corresponds to a tangent plane, this gives us a one-parameter family of tangent planes at the given point (x_0, y_0, u_0). The envelope of a family of curves (or surfaces) is defined as a curve (or surface) which has the property that at each point, it has a tangent line (or tangent plane) in common with one of the members of the family of curves (or surfaces). The envelope of the one-parameter family of the tangent planes to a surface at a fixed point is a cone called the Monge cone [1]. The intersection of any two tangent planes is a straight line which lies in the direction of the Monge cone.

Consider two "adjacent" tangent planes corresponding to:

$\lambda_1 = \lambda \qquad \lambda_2 = \lambda + \Delta\lambda$

The cross product $\vec{n}\left(\lambda_2\right) \times \vec{n}\left(\lambda_1\right)$ must lie in the direction of the Monge cone.

$$\vec{n}\left(\lambda_2\right) \times \vec{n}\left(\lambda_1\right) = \vec{n}\left(\lambda + \Delta\lambda\right) \times \vec{n}\left(\lambda\right)$$

$$\begin{vmatrix} \vec{i} & \vec{j} & \vec{k} \\ p\left(\lambda + \Delta\lambda\right) & q\left(\lambda + \Delta\lambda\right) & -1 \\ p\left(\lambda\right) & q\left(\lambda\right) & -1 \end{vmatrix} = \begin{pmatrix} q\left(\lambda\right) - q\left(\lambda + \Delta\lambda\right) \\ p\left(\lambda + \Delta\lambda\right) - p\left(\lambda\right) \\ p\left(\lambda + \Delta\lambda\right) \cdot q\left(\lambda\right) - q\left(\lambda + \Delta\lambda\right) \cdot p\left(\lambda\right) \end{pmatrix}$$

$$\lim_{\Delta\lambda \to 0} \frac{\vec{n}\left(\lambda_2\right) \times \vec{n}\left(\lambda_1\right)}{\Delta\lambda} = \begin{pmatrix} -q'\left(\lambda\right) \\ p'\left(\lambda\right) \\ p'\left(\lambda\right) q\left(\lambda\right) - q'\left(\lambda\right) p\left(\lambda\right) \end{pmatrix}$$

This last vector is called the generator of the Monge cone, which we denote as $\vec{T}\left(\lambda\right)$. At the given point (x_0, y_0, u_0), our initial equation is:

$F(x_0, y_0, u_0, p(\lambda), q(\lambda)) = 0$

Differentiating this equation with respect to λ, yields:

$$F_p p'\left(\lambda\right) + F_q q'\left(\lambda\right) = 0$$

and so:

$$\left(F_p, F_q\right) \cdot \left(p'\left(\lambda\right), q'\left(\lambda\right)\right) = 0$$

From this, we can deduce that the vectors $\begin{pmatrix} F_p \\ F_q \end{pmatrix}$ and $\begin{pmatrix} p'\left(\lambda\right) \\ q'\left(\lambda\right) \end{pmatrix}$ are perpendicular to each other, since their dot product is zero. Therefore, we know that:

$$\begin{pmatrix} p'\left(\lambda\right) \\ q'\left(\lambda\right) \end{pmatrix} = c\left(\lambda\right) \begin{pmatrix} F_q \\ -F_p \end{pmatrix}$$

The generator of the Monge cone then becomes:

$$\vec{T}(\lambda)=\begin{pmatrix}-q'(\lambda)\\ p'(\lambda)\\ p'(\lambda)q(\lambda)-q'(\lambda)p(\lambda)\end{pmatrix}=c(\lambda)\begin{pmatrix}F_p\\ F_q\\ pF_p+qF_q\end{pmatrix}$$

$\vec{T}(\lambda)$ is therefore parallel to $\begin{pmatrix}F_p\\ F_q\\ pF_p+qF_q\end{pmatrix}$.

At each point on the integral surface, there is a Monge cone with a generator direction independent of λ. This gives us a field of Monge cones. The integral trajectory through the generators is called a characteristic curve, C, defined by the equations: $x=x(\tau),\ y=y(\tau),\ u=u(\tau)$, where τ parametrizes the curve. At each point on the curve, the tangent vector must be proportional to the generator of the Monge cone. Without loss of generality, we can require that they be equal:

$$\begin{pmatrix}\frac{dx}{d\tau}\\ \frac{dy}{d\tau}\\ \frac{du}{d\tau}\end{pmatrix}=\begin{pmatrix}F_p\\ F_q\\ pF_p+qF_q\end{pmatrix}$$

We obtain two more equations by differentiating the initial equation (1) with respect to x and y, respectively:

$$\begin{aligned}&F_{x.}+F_u u_x+F_p u_{xx}+F_q u_{xy}=0\\ &F_y+F_u u_y+F_p u_{xy}+F_q u_{yy}=0\end{aligned}. \quad (2)$$

However, since $p(\tau)=u_x(x(\tau),\ y(\tau))$, and $q(\tau)=u_y(x(\tau),\ y(\tau))$,, we obtain:

$$\begin{aligned}\frac{dp}{d\tau}&=u_{xx}F_p+u_{xy}F_q\\ \frac{dq}{d\tau}&=u_{xy}F_p+u_{yy}F_q\end{aligned}$$

Substituting these into the equations (2), we obtain:

$$\begin{aligned}\frac{dp}{d\tau}&=-\left(F_x+F_u u_x\right)\\ \frac{dq}{d\tau}&=-\left(F_y+F_u u_y\right)\end{aligned}$$

We now have the following five equations:

$$\begin{aligned}\frac{dx}{d\tau}&=F_p\\ \frac{dy}{d\tau}&=F_q\\ \frac{du}{d\tau}&=pF_p+qF_q\\ \frac{dp}{d\tau}&=-\left(F_x+F_u p\right)\\ \frac{dq}{d\tau}&=-\left(F_y+F_u q\right)\end{aligned} \quad (3)$$

At each point on the characteristic curve, the quantities p and q define a tangent plane. This gives us a characteristic strip, defined by the five functions:

$x=x(\tau),\ y=y(\tau),\ u=u(\tau),\ p=p(\tau),\ q=q(\tau)$

The integral surface can be constructed from the characteristic strips from an initial curve, Γ, which is chosen in such a way that it lies on the surface. It can be parameterized as $x=x(s),\ y=y(s),\ u=u(s)$. The initial curve must obey the equation (1) of the surface:

$F(x(s),\ y(s),\ u(s),\ p(s),\ q(s))=0$

In addition, the tangent vector to the initial curve must be perpendicular to the normal vector, so:

$$\left(\frac{dx}{ds},\frac{dy}{ds},\frac{du}{ds}\right)\cdot\left(p(s),q(s),-1\right)=0$$

$$p(s)\cdot\frac{dx}{ds}+q(s)\cdot\frac{dy}{ds}=\frac{du}{ds}$$

This gives us two equations for the initial curve Γ:

$$F\left(x(s),y(s),u(s),p(s),q(s)\right)=0 \quad (4)$$

$$p(s)\cdot\frac{dx}{ds}+q(s)\cdot\frac{dy}{ds}=\frac{du}{ds} \quad (5)$$

Starting with the equations (4) and (5) of the initial curve and then integrating the equations (3) of the characteristic strip, we obtain a parametrization $x=x(s,\ \tau)$, $y=y(s,\ \tau),\ u=u(s,\ \tau),\ p=p(s,\ \tau),\ q=q(s,\ \tau)$ of the integral surface. In some cases, we may be able to eliminate s and τ and write u as a function of x and y only.

Generalization to n variables

The method described above can be extended to the case of a function of any number of variables [1]:

$u=u(x_1,\ x_2,\ ...,\ x_n)$

Consider a first-order PDE:

$F(x_1,\ x_2,\ ...,\ x_n,\ u,\ p_1,\ p_2,\ ...,\ p_n)=0$ (6)

where

$$p_1=\frac{\partial u}{\partial x_1},p_2=\frac{\partial u}{\partial x_2},...,p_n=\frac{\partial u}{\partial x_n}$$

In analogy with the equation (5) given previously, it can be shown that for any $m<n$,

$$\frac{\partial u}{\partial s_m}=p_1\left(s_1,s_2,...,s_{n-1}\right)\frac{\partial x_1}{\partial s_m}+...+p_n\left(s_1,s_2,...,s_n\right)\frac{\partial x_n}{\partial s_m}$$

Also, for any $k=1,\ 2,\ ...,\ n$, equations (3) generalize to

$$\begin{aligned}\frac{\partial x_k}{\partial\tau}&=F_{p_k}\\ \frac{\partial p_k}{\partial\tau}&=-\left(F_{x_k}+p_k F_u\right)\end{aligned}$$

and:

$$\frac{\partial u}{\partial\tau}=p_1F_{p_1}+p_2F_{p_2}+...+p_nF_{p_n}$$

This allows us to find the solution

$x_k\left(s_1, s_2, ..., s_n, \tau\right), u\left(s_1, s_2, ..., s_n, \tau\right), p_l\left(s_1, s_2, ..., s_n, \tau\right)$

where $k,\ l = 1,\ 2,\ ...,\ n$, of the equation (6).

The Equation

The equation we are considering is a special case of the Navier-Stokes equation [2], [3],

$$\vec{u}_t + \left(\vec{u} \cdot \vec{\nabla} u\right)\vec{u} = -\frac{\vec{\nabla} P}{\rho} + \nu \vec{\nabla}^2 \vec{u}$$

where $\vec{u} = \left(u_1\left(t\right), u_2\left(t\right)\right)$ is the velocity of a fluid, P is the pressure, ρ is the density, and ν is the viscosity. Equation (6) arises from making the following assumptions:

i. $\vec{u} = \left(u, u^2\right)$ for some function $u(t)$

ii. The fluid is isobaric $\vec{\nabla} P = 0$

iii. The fluid is inviscid $(\nu = 0)$

The original equation now becomes the system:

$$u_{1,t} + \left(u_1 \partial_x + u_2 \partial_y\right) u_1 = 0$$
$$u_{2,t} + \left(u_1 \partial_x + u_2 \partial_y\right) u_2 = 0$$

Which reduces to:

$$u_t + u u_x + u^2 u_y = 0 \qquad (7)$$

This is the specific equation that we study.

Applying the Method of Characteristic Strips to the Equation

We consider the equation

$$u_t + u u_x + u^2 u_y = 0$$

where $u = u(t,\ x,\ y)$ is the solution to the equation, a hypersurface in R^4 which depends on the three independent variables $t,\ x$ and y.

Let:

$t = x_1 \quad x = x_2 \quad y = x_3 \quad p_1 = u_t \; p_2 = u_x \; p_3 = u_y$

Then, we have:

$u(t,\ x,\ y) = u(x_1,\ x_2,\ x_3)$

and

$F(x_1,\ x_2,\ x_3,\ u,\ p_1,\ p_2,\ p_3) = p_1 + u p_2 + u^2 p_3 = 0$

On the initial 2-dimensional manifold, consider the following arbitrary initial conditions:

$x_1(s_1,\ s_2,\ 0) = \alpha \qquad x_2(s_1,\ s_2,\ 0) = \beta \qquad x_3(s_1,\ s_2,\ 0) = \gamma$
$u(s_1,\ s_2,\ 0) = \delta$

where α, β, γ and δ are functions of s_1, and s_2 (but not τ since τ is fixed at 0). For example, $\alpha = s_1^2 - s_2$ could be an initial condition for x_1.

Using our equation,

$F(x_1,\ x_2,\ x_3,\ u,\ p_1,\ p_2,\ p_3) = p_1 + u p_2 + u^2 p_3 = 0,$

we can obtain the equations of the characteristic strips:

$$\frac{\partial x_1}{\partial \tau} = F_{p1} = 1$$
$$\frac{\partial x_2}{\partial \tau} = F_{p2} = u$$
$$\frac{\partial x_3}{\partial \tau} = F_{p3} = u^2$$

$$\frac{du}{d\tau} = p_1 F_{p_1} + p_2 F_{p_2} + p_3 F_{p_3} = p_1 + u p_2 + u^2 p_3 = 0$$

$$\frac{\partial p_1}{\partial \tau} = -F_{x_1} - F_u p_1$$
$$\frac{\partial p_2}{\partial \tau} = -F_{x_2} - F_u p_2$$
$$\frac{\partial p_3}{\partial \tau} = -F_{x_3} - F_u p_3$$

We can integrate these equations to get $x_1,\ x_2,\ x_3$ and u as functions of the parameters $s_1,\ s_2$ and τ. In the case of equation (7), we need not first obtain $p_1,\ p_2$ and p_3 as functions of $s_1,\ s_2$ and τ, since they are not needed in order to integrate the equations for $x_1,\ x_2,\ x_3$ and u. Therefore, we can disregard these last three equations above.

Integrating the equations for u, we get:

$$\frac{du}{d\tau} = 0$$
$$\int du = \int 0 d\tau$$
$$u\left(s_1, s_2, \tau\right) = g\left(s_1, s_2\right)$$

where $g(s_1,\ s_2)$ is some arbitrary function of s_1 and s_2.

To find this arbitrary function, we can replace $\tau = 0$ and use the initial conditions:

$$u\left(s_1, s_2, 0\right) = g\left(s_1, s_2\right) = \delta$$
$$u\left(s_1, s_2, \tau\right) = \delta$$

We repeat this process for $x_1,\ x_2$ and x_3:

For x_1:

$$\frac{dx_1}{d\tau} = 1$$
$$\int dx_1 = \int d\tau$$
$$x_1\left(s_1, s_2, \tau\right) = \tau + f\left(s_1, s_2\right)$$
$$x_1\left(s_1, s_2, 0\right) = 0 + f\left(s_1, s_2\right) = \alpha$$
$$x_1\left(s_1, s_2, \tau\right) = \tau + \alpha$$

For x_2:

$$\frac{dx_2}{d\tau} = u$$
$$dx_2 = u d\tau = \delta d\tau$$
$$\int dx_2 = \int \delta d\tau$$

We can pull the δ outside of the integral since it does not depend on τ (it can only be a function of s_1 and s_2).

$$\int dx_2 = \delta \int d\tau$$
$$x_2\left(s_1, s_2, \tau\right) = \delta\tau + h\left(s_1, s_2\right)$$
$$x_2\left(s_1, s_2, 0\right) = h\left(s_1, s_2\right) = \beta$$
$$x_2\left(s_1, s_2, \tau\right) = \delta\tau + \beta$$

For x_3:

$$\frac{dx_3}{d\tau} = u^2$$
$$dx_3 = u^2 d\tau = \delta^2 d\tau$$
$$\int dx_3 = \int \delta^2 d\tau = \delta^2 \int d\tau$$
$$x_3\left(s_1, s_2, \tau\right) = \delta^2\tau + i\left(s_1, s_2\right)$$
$$x_3\left(s_1, s_2, 0\right) = i\left(s_1, s_2\right) = \gamma$$
$$x_3\left(s_1, s_2, \tau\right) = \delta^2\tau + \gamma$$

We now have x_1, x_2, x_3 and u as functions of s_1, s_2 and τ:

$$x_1 = \tau + \alpha$$
$$x_2 = u\tau + \beta$$
$$x_2 = u^2\tau + \gamma$$
$$u = \delta \tag{8}$$

The last step is to obtain u as a function of x_1, x_2 and x_3. To do this, we must choose suitable initial conditions and solve the system in a way such that we obtain an expression for δ in terms of x_1, x_2 and x_3. Several trials and observations eventually led us to identify the following solutions.

Two-Variable Solutions

One observation is that there exist several two-variable solutions to our equation. Notably,

i. If $\beta = \alpha\delta$, then:

$$\frac{x_2}{x_1} = \frac{\delta\tau + \beta}{\tau + \alpha} = \delta\frac{\tau + \frac{\beta}{\delta}}{\tau + \alpha} = \delta\frac{\tau + \alpha}{\tau + \alpha} = \delta = u$$

Therefore, with the condition that $\beta = \alpha\delta$,

$$u\left(t, x\right) = \frac{x}{t}$$

ii. If $\gamma = \beta\delta$, then

$$\frac{x_3}{x_2} = \frac{\delta^2\tau + \gamma}{\delta\tau + \beta} = \frac{\delta^2}{\delta}\frac{\tau + \frac{\gamma}{\delta^2}}{\tau + \frac{\beta}{\delta}} = \delta\frac{\tau + \frac{\beta}{\delta}}{\tau + \frac{\beta}{\delta}} = \delta = u$$

Therefore, with the condition that $\gamma = \beta\delta$:

$$u\left(x, y\right) = \frac{y}{t}$$

iii. If $\gamma = \alpha\delta^2$, then

$$\sqrt{\frac{x_3}{x_1}} = \sqrt{\frac{\delta^2\tau + \gamma}{\tau + \alpha}} = \delta\sqrt{\frac{\tau + \frac{\gamma}{\delta^2}}{\tau + \alpha}} = \delta\sqrt{\frac{\tau + \alpha}{\tau + \alpha}} = \delta = u$$

Therefore, with the condition that $\gamma = \alpha\delta^2$:

$$u\left(t, y\right) = \sqrt{\frac{y}{t}}$$

Three-Variable Cubic Solution

If we choose $\alpha = 0$, $\beta = s_1$, $\gamma = s_2$, and $\delta = \frac{s_1}{s_2}$, the system then becomes:

$$x_1 = \tau$$
$$x_2 = \frac{s_1}{s_2}\tau + s_1$$
$$x_3 = \frac{s_1^2}{s_2^2}\tau + s_2$$
$$u = \frac{s_1}{s_2}$$

From the second equation in the system, we get:

$$s_1 = \frac{x_2}{\frac{\tau}{s_2} + 1}$$

So:

$$s_1 = \frac{x_2}{\frac{x_1}{s_2} + 1} = \frac{s_2 x_2}{x_1 + s_2}$$

Replacing this expression for s_1 in the third equation, we obtain

$$x_3 = \frac{1}{s_2^2}\left(\frac{s_2 x_2}{x_1 + s_2}\right)^2 \tau + s_2$$

which leads to the equation for s_2:

$$s_2^3 + s_2^2\left(2x_1 - x_3\right) + s_2\left(x_1^2 - 2x_1 x_3\right) + \left(x_1 x_2^2 - x_1^2 x_3\right) = 0$$

We can use Cardano's formula to obtain an expression for s_2 in terms of x_1, x_2, and x_3:

$$s_2 = \frac{1}{6}\left(-108q + 12\sqrt{12p^3 + 81q^2}\right)^{\frac{1}{3}} - \frac{2p}{\left(-108q + 12\sqrt{12p^3 + 81q^2}\right)^{\frac{1}{3}}} - \frac{b}{3}$$

where

$$b = 2x_1 - x_3$$
$$c = x_1^2 - 2x_1 x_3$$
$$d = x_1 x_1^2 - x_1^2 x_3$$

$$p = \frac{3c - b^2}{3}$$

$$q = \frac{2b^3 - qbc + 27d}{27}$$

Since $u\left(x_1, x_2, x_3\right) = \frac{x_2}{x_1 + s_2}$, we obtain the following solution

$$u\left(t, x, y\right) = \frac{x}{t + s_2}$$

where s_2 is given by the formula above

Three-Variable Solution in Explicit Form

Consider the case where $\alpha = 0$, $\beta = \gamma = s_2$, and $\delta = s_1$. The system then becomes:

$$\begin{aligned} x_1 &= \tau \\ x_2 &= s_1\tau + s_2 \\ x_3 &= s_1^2\tau + s_2 \\ u &= s_1 \end{aligned} \tag{10}$$

Subtracting the third equation from the second, we obtain:

$$\begin{aligned} x_2 - x_3 &= s_1\tau - s_1^2\tau \\ 0 &= s_1^2 x_1 - s_1 x_1 + \left(x_2 - x_3\right) \end{aligned}$$

We now have a quadratic expression for s_1 involving only x_1, x_2, and x_3. Using the quadratic formula, we get:

$$s_1 = u\left(x_1, x_2, x_3\right) = \frac{x_1 \pm \sqrt{x_1^2 - 4x_1\left(x_2 - x_3\right)}}{2x_1}$$

$$u\left(t, x, y\right) = \frac{t \pm \sqrt{t^2 - 4tx + 4ty}}{2t} = \frac{1}{2} \pm \sqrt{\frac{1}{4} - \frac{x}{t} + \frac{y}{t}}$$

Note: we can observe that there are, in fact, infinitely many quadruplets $(\alpha, \beta, \gamma, \delta)$ that will yield this solution, as long as $\alpha = 0$ and $\beta = \gamma$.

References

1. R. Courant and D. Hilbert, *Methods of Mathematical Physics*, Volume 2, John Wiley and Sons, New York, 1962. (For the method of Characteristic Strips).
2. L.D. Landau and E.M. Lifshitz, *Fluid Mechanics*, 2nd edition, Elsevier, 2004. (Navier-Stokes equation).
3. A. M. Grundland and P.J. Vassiliou, On the solvability of the Cauchy problem for Riemann double-waves by the Monge-Darboux method, *Analysis*, 11, 221-278, 1991. (Our equation was used as an example to illustrate the Cauchy problem for Riemann double-waves).

An Application of the Least Residue System Modulo 4

Dragos Secrieru

Abstract

The following paper gives a partial result to the problem of finding all integers n for which $a+2^n$ is a perfect square, with a being a fixed integer. Additionally, multiple questions are posed inspired by the original problem.

Introduction

The following solution will rely heavily on modular arithmetic with special attention given to mod 4. A number is said to be in mod 4 if it is written in the form $4k + l$, where k is an integer and $l = (0, 1, 2, 3)$ are the possible remainders. The reasoning behind the usage of modular arithmetic is that if a solution is found for a specific remainder, we then have an infinite set of numbers for which a solution exists. The following solution classifies all the possible remainders. If a solution is found, then modular arithmetic will provide us with an infinite number of solutions.

Problem The problem, first introduced by professor Ohanyan at the beginning of the 2018 Winter semester, has 2 parts:

Part 1: For which integer values of n, is the number $7+ 2^n$ a perfect square?

Part 2: Let a be any fixed integer. For which integer values of n is $a + 2^n$ a perfect square?

Result: For a's of the form $4m +2$ and $4m +3$ there exists a finite number of n's for which the expression forms a perfect square, provided that n is either 1 or 2. For a's of the form $4m$ and $4m +1$ there exists infinitely many n's for which a solution exists.

Moreover, when a is of the form $4m$, n is finite if x is odd. Similarly, for $4m + 1$, n is finite if x is even. In all other cases n is infinite.

1. Part One

It is clear to see that $n =1$ is a possible solution. The goal of the paper is to determine whether there are solutions for other values of n as well.

Let us reformulate the equation of Part 1 $(7 + 2^n = x^2)$, in the following way:

1.1 RHS

If x is even, then $x^2 = (2k_1)^2 = 4k_1^2 = 4k_2$.

If x is odd, then $x^2 = (2k_3 + 1)^2 = 4k_3^2 + 4k_3 + 1 = 4(k_3^2 + k_3) + 1 = 4k_4 + 1$. Therefore, x^2 is either of the form $4k$ or $4k + 1$.

1.2 LHS

If $n \geq 2$, 2^n is always of the form $4l$, and 7 is simply of the form $4m + 3$.

1.3 First case (x is even)

If $4m + 3 + 2^n = 4k$, then the RHS is even, which implies that the LHS is also even. The LHS is even if and only if 2^n is odd, which only happens when $n = 0$.

1.4 First case (x is odd)

If x is odd, then $4m +3 + 2^n = 4k + 1$. Therefore, for $n \geq 2$, there are no possible solutions since 2^n is of the form $4l$. The only two remaining cases are now when $n \in \{0, 1\}$. However, there is clearly no solution when $n = 0$, which means the only possible case where a solution may exist is when $n = 1$.

So far, we have considered the case where a is of the form $4m + 3$, which means that the possible solutions for this case are of the form $(a, n) = (4m + 3, \{0, 1\})$.Therefore $n =1$ is the only possible solution for Part 1.

2. Part Two

The case $a = 4m + 3$ has been described above, the three remaining cases are: $4m$, $4m +1$ and $4m + 2$.

2.1 $(4m + 2)$

Case 1: If x is even and $a = 4m + 2$, then $4m +2 + 2^n = 4k$. By the same method as in Part 1, we can see that the solutions exist if and only if $n = 1$.

Case 2: If x is odd then $4m +2+ 2^n = 4k + 1$. Regardless of the value of n, it is impossible for 2^n to attain the form of $4l + 3$. Consequently, there is no solution. Therefore, the possible solutions will have the form $(a, n) = (4m + 2, \{1\})$ with $m \in \{0, 3, 8, 15, 24, ...\}$ and $k \in \{4, 9, 16, 25, ...\}$.

2.2 ($4m$ and $4m + 1$)

Since x^2 takes two possible forms in mod 4, we have a total number of four possible combinations of a and x^2.

$4m + 2^n = 4k$ $\qquad$ $4m + 2^n = 4k + 1$

$4m + 1 + 2^n = 4k$ $\qquad$ $4m +1 + 2^n = 4k + 1$

Case 1:

$4m + 2^n = 4k$

$2^n = 4(k - m)$

which means $n \in \{2, 3, 4, 5...\}$. To categorize all possible solutions, replace x^2 with $4k_1^2$

$4m + 2^n = 4k_1^2$

$4m = 4k_1^2 - 2^n$

$m = k_1^2 - 2^{n-2}$

This gives us the following solutions:

$(n,\ k_1,\ m)$

$(2,\ 1,\ 0), (2,\ 2,\ 3), (2,\ 3,\ 8), \ldots, (2,\ i,\ i^2 - 1)$

$(3,\ 2,\ 2), (3,\ 3,\ 7), (3,\ 4,\ 14), \ldots, (3,\ i,\ i^2 - 2)$

$\vdots \quad \vdots \quad \vdots \quad \vdots$

Case 2:

$4m + 2^n = 4k + 1$

$n = 0$

The possible solutions will have the form $(a,\ n) = (4m,\ \{0\})$ with $m \in \{0,\ 2,\ 6,\ 12,\ 20,\ \ldots\}$.

Case 3:

$4m + 1 + 2^n = 4k$ (no solutions)

Case 4:

$4m + 1 + 2^n = 4k + 1$

$4m + 2^n = 4k$

Note that Case 4 is not the same as Case 1, since in Case 4, x^2 is of the form $4k_2^2 + 4k_2 + 1$ and not $4k_1^2$.

$4m + 1 + 2^n = 4k_2^2 + 4k_2 + 1$

$4m + 2^n = 4k_2^2 + 4k_2$

$m = k_2^2 + k_2 - 2^{n-2}$

This gives us the following solutions:

$(n,\ k_2,\ m)$

$(2,\ 1,\ 1), (2,\ 2,\ 5), (2,\ 3,\ 11), \ldots, (2,\ i,\ i^2 + i - 1)$

$(3,\ 1,\ 0), (3,\ 2,\ 4), (3,\ 3,\ 11), \ldots, (3,\ i,\ i^2 + i - 2)$

$\vdots \quad \vdots \quad \vdots \quad \vdots$

3. Additional statements

Lemma 3.1. If x is not a multiple of 3 then $x^2 - 2^{2k} = 3l$.

Proof.

$x^2 - 2^{2k} \equiv 3l$ (mod 3)

$x^2 - 2^{2k} \equiv 0$ (mod 3)

$(x + 2^k)\ (x - 2^k) \equiv 0$ (mod 3)

There are two possible values for x: $3l + 1$ and $3l + 2$.

Case 1: $(3l + 1)$

Since 3 is not a power of 2, then the only possible values for a in the equation $2^{2k} \equiv a$ (mod 3) are 1 and 2.

$(3l + 1 + 2^k)(3l + 1 - 2^k) \equiv 0$ (mod 3)

By letting 2^k equal 1 and 2, we notice that in each case we get a multiple of 3, making it divisible by 3.

Case 2: $(3l + 2)$

$(3l + 2 + 2^k)(3l + 2 - 2^k) \equiv 0$ (mod 3)

By letting 2^k equal 1 and 2, we notice that in each case we get a multiple of 3, making it also divisible by 3.

Lemma 3.2. For all prime values of p except 3, $p^2 - 2^3 = 3l + 2$ (l is an integer).

Proof.

$p^2 - 8 \equiv 3l + 2$ (mod 3)

$p^2 \equiv 1$ (mod 3)

$(p - 1)(p + 1) \equiv 0$ (mod 3)

If p is either of the form $3k + 1$ or $3k + 2$ then $(p - 1)(p + 1)$ is a multiple of 3. Note that if $p = 3$ then $(p - 1)(p + 1)$ is not a multiple of 3.

3.1 Additional question

Lemma 3.1 $(x^2 - 2^{2k} = 3l)$ can be combined with the reformulated Lemma 3.2 $(p^2 - 10 = 3m)$, or even $p^2 - 1 = 3l$. Combining Lemma 3.1 and 3.2, a question arises:

Question: Find all possible triples $(x,\ k,\ p)$, p being prime and x, k being integers, for which $x^2 - 2^{2k} = p^2 - 1$.

4. Unproven statements

We look at $(a,\ n)$ of the form $a + 2^n \equiv 0$ (mod p), where p is prime. The notation used for mods will be given in parentheses.

$a + 2^n \equiv 0$ (3), $a + 2^n \equiv 0$ (5), $a + 2^n \equiv 0$ (7),

$a + 2^n \equiv 0$ (11), $a + 2^n \equiv 0$ (17), $a + 2^n \equiv 0$ (31)

n	a (3)	a (5)	a (7)	a (11)	a (17)	a (31)
0	2	4	6	10	16	30
1	1	3	5	9	15	29
2	2	1	3	7	13	27
3	1	2	6	3	9	23
4	...	4	...	6	1	15
5	...	...	...	1	2	30
6	...	...	...	2	4	...
7	...	...	...	4	8	...
8	...	...	...	8	16	...
9	...	...	...	5	...	...
10	...	...	...	10	...	...
11	...	...	...	...	...	...

We note the periodicity of the solutions. For example, the periodicity of 3 is 2, of 5 is 4, of 11 is 10, of 31 is 5. This means that for a prime p, the periodicity is $p - 1$ except for the values: 7, 17, 31, 89, 127... It is interesting to note that these numbers are Mersenne exponents, meaning they satisfy the following equation, where p and q are primes:

$2^p - 1 = q$

The presence of the numbers 7, 31 and 127 can be explained by the fact that they can all be written as $2^k - 1$, where k is an integer. It is then trivial to show why they don't follow the $p - 1$ rule.

As a consequence of our analysis, two questions arise:

1. Does every single prime number have a periodicity?
2. Does there exist a function $f(p)$ which gives the periodicity of that prime?

Another interesting problem would be to find a pattern for a in the equation $a + 2^n = p^2$, for all prime numbers p for a given integer n.

The Effect of Musical Background on the McGurk Effect in Younger and Older Adults

Eri Kajita, Alexander Ngo, Angely Te and Rajesh Malik

Abstract

The McGurk effect is an audio-visual illusion that is produced when an auditory stimulus is mismatched with a visual stimulus producing a completely different perceptual experience. In our study, we researched the degree of the effect on musicians compared with non-musicians and hypothesized that the latter would be more susceptible to the effect for reason that having a musical background would lead to developed hearing, which would reduce the chances of experiencing the illusion. We also hypothesized that the alternation of the vowels from aa to ii, would increase the likelihood of participants undergoing the illusory effect, based on past studies. On the other hand, flipping the auditory stimulus with the visual stimulus would reduce the likelihood of experiencing the McGurk effect. We also predicted that older adults would be more likely to experience the effect.

There was a total of 96 participants including 19 elderly and 77 young adults, of which 28 were musicians, who took part in the study.

The results were not significant, however it showed that the McGurk effect was experienced less among those who have a musical background as opposed to those who do not. Participants were also more susceptible to the illusion with vowels ending in ii than those ending with aa. Although the results were not significant, the trends were in the right direction. The results for flipping the audio ba to audio ga, and visual ga to visual ba led to a reduction in the Mcgurk effect. Finally, our research concluded that the elderly experienced the McGurk effect more than young adults.

Introduction

The McGurk effect is a perceptual illusion that supports a model in which the brain is multimodal. In other words, the brain has the ability to combine sensory systems to perceive information. The Superior Temporal Sulcus (STS) is the area of the brain that is responsible for the perception of the McGurk effect (Beauchamp, et al., 2010). This illusion occurs when an auditory stimulus is presented simultaneously with an incongruent visual stimulus, leading to the perception of an entirely different speech interpretation. For instance, when the auditory stimulus Ba is presented with the visual stimulus Ga, the result generates the perception of Da. In other words, we presented the participant with a video of a pair of lips that was superimposed with a mismatched audio. Depending on the participant, the participant's brain will register both the auditory and visual component of the effect as one and then perceive a combination of both syllables, a completely different syllable, or just the audio sound. Another example used the stimuli Pa and Ka to be perceived as Ta (McGurk & MacDonald, 1976). Studies have shown that the McGurk effect is experienced in a variable manner, with a wide range of 15% to 98% of the population experiencing the illusion (Alsius, et al. 2016). Also, individuals who experience the McGurk effect will always be susceptible to the illusion despite their awareness of the audio-visual phenomenon taking place. This is due to the fact that the brain consistently integrates the stimuli under that effect (McGurk, and MacDonald, 1976).

There are many factors that contribute to the degree to which the McGurk effect is experienced, such as gender, age and musical training, to name a few.

Older adults are more susceptible to the McGurk effect due to their different brain organization (Setti, A., et al. 2013). Hence, there is a correlation between age and the susceptibility to the audio-visual phenomenon.

Another factor that affects the perceptibility of the McGurk effect is musical background. According to certain studies, having previous musical training decreases the likelihood of the perception of the McGurk effect (Proverbio, A. M., et al., 2016). In this study, eighty healthy graduate male and female volunteers were individually subjected to a few tests. These tests consisted of an auditory simulation with a blank screen, a visual stimulation without sound, and a combined audiovisual simulation. There was a total of 40 participants, 15 of whom were female are 35 male, with a range of 13 to 18 years of musical experience, excluding musical training with their voice. They discovered that the McGurk effect was experienced to a significantly reduced degree when compared to 40 participants of comparable age with a lack of musical background.

A study from Japan found that the McGurk effect was experienced to different degrees depending on the ending vowel context (Shigeno, S., 2000). While most studies use the vowel /a/ when studying the McGurk effect, this study shows that the vowels with the largest influence on the perception of the illusion are stimuli that end with /i/, followed by /a/, and with nearly no influence on the effect are vowels ending in /u/. In conjunction to altering different parts of the stimulus, a study also found that reverse dubbing an audiovisual stimuli alters the perceived syllable (McGurk, H. and MacDonald, J. 1976).

From fMRI scans, numerous regions of the brain have been associated with interpreting speech perception. These include regions such as the inferior parietal lobule (Jones and Callan, 2003), the precentral gyrus (Jones and Callan,

2003), the superior frontal gyrus (Miller and D'Esposito, 2005), and Heschl's gyrus (Miller and D'Esposito, 2005), among many others. However, transcranial magnetic stimulation (TMS) has shown that another area of the brain, located at the superior temporal sulcus (STS), is critical for interpreting the McGurk effect (Beauchamps, et al. 2010). When the TMS was delivered to the STS within a +/-100 ms window of the auditory stimulus, the McGurk effect was less likely to be perceived (Beauchamp, et al. 2010).

With further research on the McGurk effect, scientists are hoping to discover the different functions of the brain and how it is comprised of many systems that work together to perceive information.

In our study, we first determined the percentage from our total sample who are susceptible to the illusion and compared this value with the wide range of McGurk responders found in other studies. Our study aims to confirm the hypotheses of previous studies based on three variables: age, musical background, and manipulation of vowels. First, it was hypothesized that McGurk effect would be experienced less among those who have a musical background than those who do not. Second, the use of certain vowels is significant to the perception of the McGurk effect, where stimuli ending in /i/ generates more McGurk responses than stimuli ending with /a/. Third, flipping the audiovisual stimuli, from audio ba visual ga to audio ga visual ba for instance, would decrease the incidence of this illusion. Last, older adults would experience this audio-visual illusion to a greater degree than younger adults.

Neuroscience Behind the McGurk Effect

An important study used fMRI to study the activity in the Superior Temporal Sulcus (STS) upon the presentation of McGurk stimuli (Beauchamp, et al. 2010). When the STS was temporarily made inactive by the transcranial magnetic stimulation (TMS), participants reported the audio part of the stimuli correctly, but no McGurk effect was observed. The study concluded that the STS may be responsible for this audio-visual illusion and may play a critical role in combining multisensory information such as visual and auditory information.

Method

Participants

Ninety-eight participants took part in the study, though two were omitted from the results as they did not accurately perceive the auditory stimuli during the practice trials. From the total, 77 participants were between 16 to 35 years, and 19 were over the age of 64. Among the participants classified as young adults, 28 were musicians. Eligibility to participate were based on the following criteria: alongside having to fit in the age range of either young adults or older adults, participants had to be fluent in English and/or French and they must have had either normal or corrected-to-normal vision. To further qualify as a musician, participants were required to have had at least three years of continuous musical training at some point in the past this includes experience with an instrument, including their voice. They should still be pursuing their training or had stopped less than a year prior to testing.

Materials

A computer was used to create a Powerpoint slideshow of the twenty four stimuli. The test was segmented into three sections: audiovisual, audio and audiovisual. The first audiovisual segment was a combination of lip movement and audio stimuli of one of the four stimuli: ba, ga, bii and gii that were presented six times to check the participants' hearing and their understanding of the exercise. The second segment consisted of six auditory stimuli played over a blank screen with a dot at the center. The third segment consisted of four incongruent audiovisual stimuli: auditory ba with visual of the lip movement of ga, auditory bii with visual gii, auditory ga with visual ba, and auditory gii paired with visual bii.

Procedure

Each participant was first asked a series of questions to see if they met the criterion for this experiment. If so, they were then introduced to the team and the procedure was explained to them. Once they agreed to participate, the consent form was signed.

Upon completing the practice trials, we randomly assigned one of the two tests that were created to present to the participant through a coin toss. Each version was comprised of the same stimuli, the only difference being the order of the stimuli presented in each segment. During the trials, participants were seated a distance of 30 cm from the computer screen. Participants were given a full debriefing at the end of the experimental session.

Results and Discussion

The first thing we checked was to what degree the participants heard what was presented during the first segment. In Figure 1, results show that most participants could correctly hear and interpret the audiovisual stimuli. With the highest mean possible being three, the stimuli run from the practice trials were heard with high accuracy among musicians, and nonmusicians. Among the elderly, however, the auditory stimulus was heard on average 2.47/3 times for stimulus bii, and 2.32/3 times for stimulus gii, with a standard deviation of 0.964 and 1.108 respectively. Although it is within acceptable range, the elevated standard deviations makes us question as to whether they heard what they were supposed to.

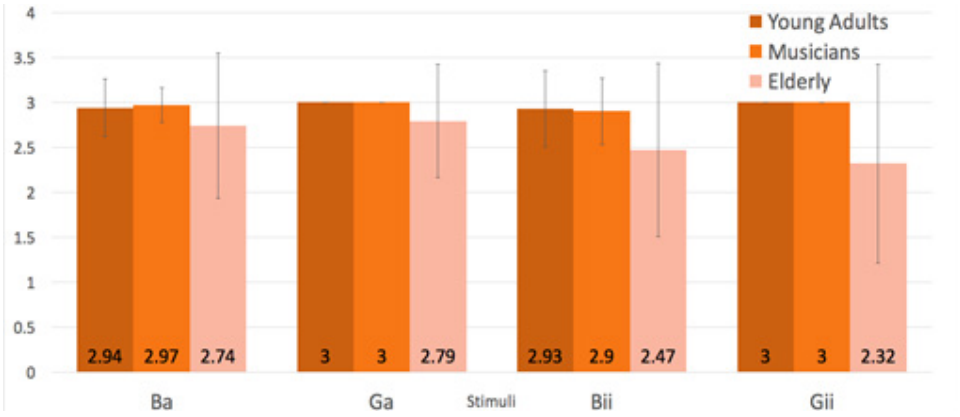

Figure 1: Mean Number of Correct Responses of auditory stimuli during practice trials for young adults, musicians and the elderly.

The results were measured in two ways. We first calculated how often the McGurk effect occurred per syllable in each of our study groups by using the following formula:

We categorized participants as McGurk responders when they experienced the McGurk effect ⅔ times when the stimulus was presented. This was done by dividing the

$$mean = \frac{Number\ of\ times\ the\ McGurk\ Effect\ was\ heard\ per\ stimulus}{Number\ of\ times\ a\ stimulus\ was\ presented}$$

By dividing the number of times the McGurk effect was heard per stimulus by the number of times that a stimulus was presented, we obtained a mean of the occurrence of the McGurk effect that was experienced per group.

Each stimulus (syllables ba, ga, bii, & gii) was presented three times in random order for each participant. Figure 2 presents the mean of McGurk responders in each study group, where we observe that the elderly experienced the illusion to a much greater degree than young adults and musicians across all four stimuli.

number of McGurk responders by the total number of participants in the sample and multiplied by one hundred. Figure 3 shows the percentage of McGurk responders in each group across the four stimuli.

A study from 2017 claimed McGurk responders range between 15% to 98% of the population (Alsius, et al. 2016). The percentage of young adults who experienced the effect in our study, found in Figure 3, is 35%, which is not as high as the study, but which still falls in the range. As for the elderly, the percentage was 74% for stimulus bii and

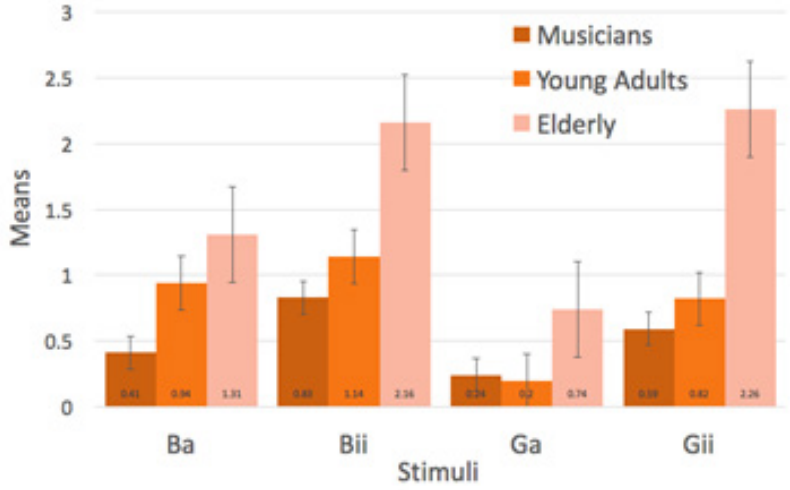

Figure 2: The mean number of McGurk responders in young adults, musicians, and the older adults across four stimuli

The second way the McGurk effect was measured was by percentage, using the following formula

80% for stimulus gii, which is a greater amount of McGurk responders than the younger adults.

$$\% = \frac{Number\ of\ times\ the\ McGurk\ responded}{Number\ of\ participant\ in\ a\ group}$$

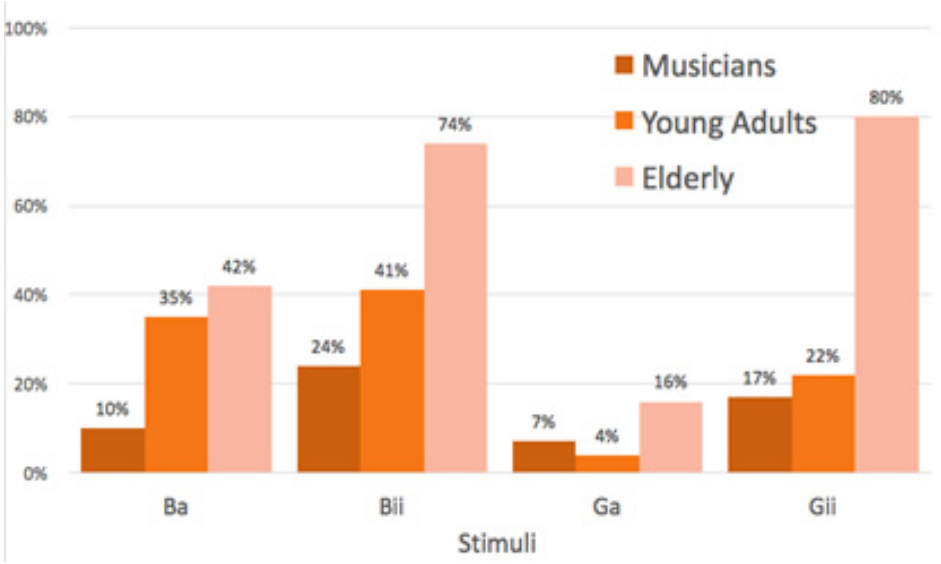

Figure 3: Percentages of McGurk responders in each group across four stimuli

Our first hypothesis was that musicians would experience the McGurk effect less than young adults. Based on our results, we can observe that non-musicians experienced the McGurk effect at least twice as much as musicians for audiovisual stimuli ba-ga and bii-gii as shown by the mean and the percentages (Figure 4). For example, non-musicians had a mean of 0.94 and a percentage of 34.7 for ba-ga, while musicians had a mean of 0.41 and a percentage of 10.3. However, it was small and non-significant for both ba-ga and bii-gii.

We stated in our second hypothesis that the McGurk effect would be experienced more with vowels ii than with vowels aa. The McGurk effect was experienced 0.94/3 for the audiovisual stimulus where the audio was ba and visual was ga among the young adults, with the most common response for the illusion as da, making 35% of the young adults McGurk responders (Figure 5). Meanwhile, the mean was 1.14 for the stimulus audio bii matched with visual gii,, with 40.8% of young adults experiencing it, while the most common heard stimulus was dii. Although the

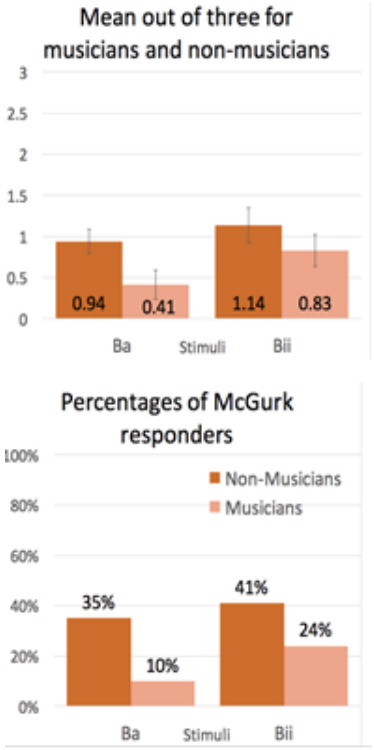

Figure 4: The mean and percentage of McGurk Responders in Non-Musicians and Musicians

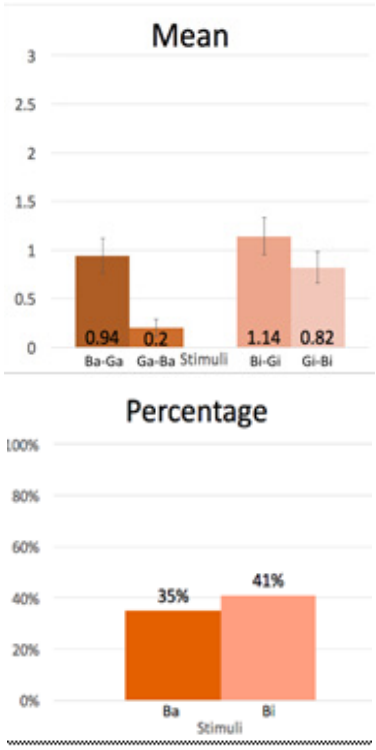

Figure 5: Differences in McGurk effect perception across different vowel ending for young adults

trends are in the right direction, we didn't find significant results using the Kruskal-Wallis test

Our following hypothesis states that flipping the stimulus would decrease the effectiveness of the McGurk effect. For instance, the incidence of the McGurk effect for the stimuli ba-ga and bii-gii would be much higher than for stimulus ga-ba and gii-bii. With a mean of 0.94 for ba-ga and 0.20 for the flipped stimulus, young adults experience ba-ga more than ga-ba. The percentages also supported the same trend. The Kruskal-Wallis test supported our hypothesis with a p-value of 0.0093. For the stimulus ba-ga, the most common heard McGurk response was da. However, for stimulus ga-ba, it was bga. Although we did not specifically make a prediction for stimulus bii-gii, the results were statistically non-significant when flipping the stimulus to *gii-bii*.

For our last hypothesis, we stated that the elderly would experience the McGurk effect more than the younger individuals because of differences in brain organization. With the Mann-Whitney U-test, the results from Figure 6 for ba-ga were statistically non-significant. In fact, the mean and percentage for young adults and the elderly was 0.94 and 34.7%, and 1.31 and 42% respectively. However, the results for the stimulus bii-gii showed that the elderly were significantly more susceptible to the McGurk effect than the young adults, with a p-value of 0.0099. The most commonly heard syllable for the elderly were aa and da for ba, dii for bii..

Conclusions

This study aimed to confirm the hypotheses inspired from the literature reviews based on the following variables: age, musical background, manipulation of vowels and flipping the presentation of stimuli.

Although, the trends were in the right direction for our hypotheses that musicians would experience the McGurk effect less than non-musicians and that vowels ending in ii would produce more McGurk responders, our research did not produce any significant results for these hypothesis. In the instance where the audio and visual stimuli was flipped, we hypothesized that the degree of experiencing the McGurk effect would be reduced. We discovered that there is a significant difference in the perception of the McGurk effect, being that the audio ba and visual ga flipped to the audio ga and visual ba, were the only vowels to produce significant results. Our final hypothesis was also partially supported, being that the elderly would experience the McGurk effect more than young adults, although it is only statistically significant with vowels ending with ii.

With further research on the McGurk effect, scientists are hoping to discover the different

functions of the brain and how it is comprised of many systems that work simultaneously together to perceive sensory information.

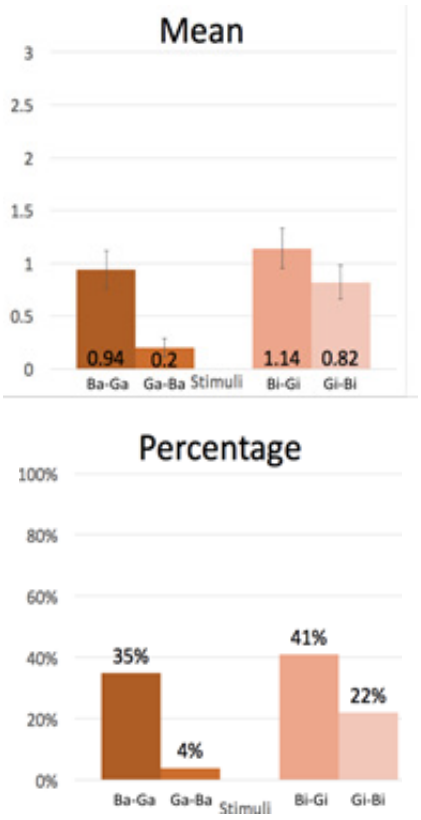

Figure 6: The perception of McGurk effect with flipped stimuli for young adults

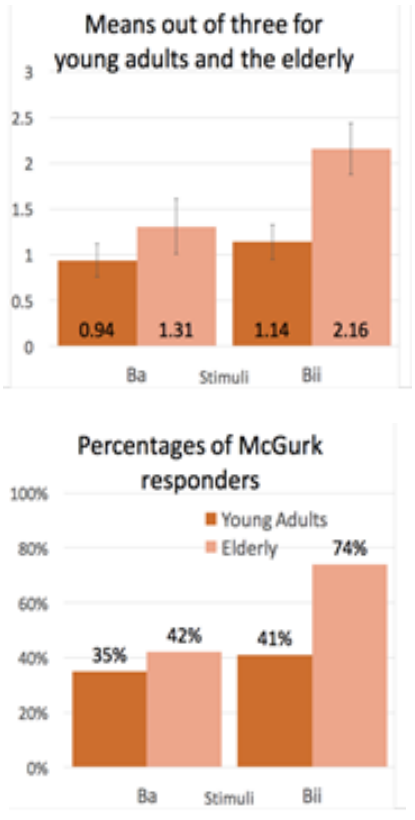

Figure 7: McGurk effect perception of young adults vs. the elderly

Limitations

Possible limitations that may have affected the results in our study may lie in our broad definition in what we used to qualify participants as being a musician. Whereas, we could have narrowed down the type of musical training required in order to be considered as a musician. Other factors could have been set in place, such as the frequency in which they play the instrument and how often they practice, in order to refine our results. Setting more strict requirements could have led to results that produced a significant difference when comparing McGurk responders in the musician category and non-musicians.

We did not employ a test to determine whether all participants had normal hearing for speech perception, and this fact could be especially relevant for the elderly as a larger standard deviation was observed for them than for the younger adults. Also, when producing the audio/visual stimuli, , some of them may not have been in complete sync. In other words, the time gap between the moment that the visual stimulus was presented was not in the +/- 100 ms window of when the auditory stimulus was presented.

Ideally, more trials should be run than what we administered, but this was out of our control because of time constraints.

References

1. Alsius, A., Paré, M., & Munhall, K.G. (2016). Forty years after hearing lips and seeing
2. voices: the McGurk effect revisited. Multisensory Research, 264 1-34. DOI: 10.1163/22134808-00002565
3. Beauchamp, M. S., Nath, A. R., & Pasalar, S. (2010). fMRI-guided transcranial magnetic
4. stimulation reveals that the superior temporal sulcus is a cortical locus of the McGurk effect. Journal of Neuroscience, 30(7), 2414-2417. DOI:10.1523/jneurosci.4865-09.2010
5. Callan DE, Jones JA, Munhall K, Kroos C, Callan AM, Vatikiotis-Bateson E (2004)
6. Multisensory integration sites identified by perception of spatial wavelet filtered visualspeech gesture information. J Cogn Neurosci 16:805– 816.
7. Mallick, D. B., Magnotti, J. F., & Beauchamp, M. S. (Oct. 2015). Variability and stability in
8. the McGurk effect: contributions of participants, stimuli, time, and response type. Psychon Bull Rev, 22(5), 1299–1307. DOI:10.3758/s13423-015-0817-4
9. Miller LM, D'Esposito M. (2005) Perceptual fusion and stimulus coincidence in the cross-modal integration of speech. J Neurosci 25:5884 –5893.
10. McGurk, H., MacDonald, J. (1976). Hearing lips and seeing voices. Nature, 264, 746-748.
11. Proverbio, A. M., Massetti, G., Rizzi, E., & Zani, A. (2016). Skilled musicians are not subject
12. to the McGurk effect. Retrieved from www.nature.com/articles/srep30423
13. Setti, A., Burke, K.E., Kenny, R., & Newell, F.N. (2013). Susceptibility to a multisensory
14. speech illusion in older persons is driven by perceptual processes. Front Psychol, 4, 575.
15. Shigeno, S. (2000). Influence of vowel context on the audio-visual speech perception of
16. voiced stop consonants. Japanese Psychological Research, 42(3), 155–167.

On a Certain Type of Universality for Real Series

Jiahao Deng and Richard Fournier

Abstract

A universality statement for real series related to the Riemann rearrangement theorem is stated and proved.

Introduction

Recall that a real series $\sum_1^\infty a_n$, that is a series with terms in the set R of real numbers, is absolutely convergent (AC) if $\sum_1^\infty |a_n|$ is convergent. It is well-known that such series are convergent. A series is conditionally convergent (CC) if it is convergent but not absolutely convergent. Any CC series $\sum_1^\infty a_n$ has a very (at first sight!) striking property: given any real number x, there exists a bijection β of the set of positive integers such that $\sum_1^\infty a_{\beta(n)} = x$; this is the famous rearrangement theorem of Bernhard Riemann [1]. This result may be interpreted as a universality statement [2]: any CC series is universal in the sense that it generates, through bijections of N, the whole real line R, in fact even the whole real line completed with the symbols $\pm\infty$.

We shall say that a series $\sum_1^\infty a_{n_j}$ is a subseries of the series $\sum_1^\infty a_n$ if $\{n_j\}$ is a subset of N. From [3], by imitating the standard proof of the Riemann's theorem, it may be shown that any divergent series $\sum_1^\infty p_n$ with positive terms tending to 0 (i.e., $\lim_n p_n = 0$ but $\sum_1^\infty p_n = \infty$) admits, given a positive number x, a subseries whose sum is precisely x; we may interpret this result as meaning that any such series $\sum_1^\infty p_n$ is universal with respect to subseries. The goal of this note is to prove the following.

Theorem: Given a CC series $\sum_1^\infty a_n$ and two real sequences $\{x_k\}$ and $\{y_k\}$ with $y_k \geq 0$, there exist subseries $\sum_1^\infty a_{n_j^{(k)}}$ and $\sum_1^\infty a_{n_{j_t}^{(k)}}$ such that for all $k \geq 1$, $\sum_1^\infty a_{n_j^{(k)}} = x_k$ and $\sum_1^\infty \left|a_{n_{j_t}^{(k)}}\right| = y_k$ and $\left\{n_j^{(k+1)}\right\} \cap \cup_{l=1}^k \left\{n_{j_t}^{(l)}\right\} = \varnothing$. The notation $\left\{n_j^{(k)}\right\}$ is used to stress the dependence of the sequence $\{n_j\}$ on the index k.

It is not clear at all what this result really means but it definitely has a universality flavor. In fact, the infinite system of equations $\sum_1^\infty a_{n_j^{(k)}} = x_k$ and $\sum_1^\infty \left|a_{n_j^{(k)}}\right| = y_k$, $k \geq 1$, (here we think of the sequences $\left\{n_j^{(k)}\right\}$ as being the unknowns) clearly has no solution if for example $|x_k| > y_k$ for at least one index k and we may therefore think of our result as being a "second best" statement.

Proof

The argument here is entirely based on the Riemann's theorem. From the beginning it may be assumed that for some real number x_0 and some positive number y_0, we have $\sum_1^\infty a_n = x_0$ and for some subsequence of integers $\left\{n_j^{(0)}\right\}$, $\sum_1^\infty \left|a_{n_j^{(0)}}\right| = y_0$ because $\sum_1^\infty a_n$ is assumed to be a CC series. Let us observe that $\sum_{n\in N-\left\{n_j^{(0)}\right\}} a_n$ is convergent because it is a difference of two convergent series but $\sum_{n\in N-\left\{n_j^{(0)}\right\}} |a_n|$ is divergent because otherwise the original series $\sum_1^\infty a_n$ would be absolutely convergent!

It follows from Riemann's theorem that for some bijection $\beta^{(1)}$ of $N - \left\{n_j^{(0)}\right\}$ we have $\sum_n a_{\beta^{(1)}(n)} = x_1$ and since $\sum_n \left|a_{\beta^{(1)}(n)}\right| = \infty$, there exists $\left\{n_j^{(1)}\right\}$ included in N - $\left\{n_j^{(0)}\right\}$ such that $\sum_j \left|a_{\beta^{(1)}\left(n_j^{(1)}\right)}\right| = y_1$. Just as above, $\sum_{n\in N-\left\{n_j^{(0)}\right\}-\left\{n_j^{(1)}\right\}} a_\eta$ is a CC series and there shall exist a bijection $\beta^{(2)}$ of N - $\left\{n_j^{(0)}\right\}$ - $\left\{n_j^{(1)}\right\}$ such that $\sum_n a_{\beta^{(2)}(n)} = x_2$. Clearly $\sum_n a_{\beta^{(2)}(n)}$ is itself a CC series and there must exist a sequence $\left\{n_j^{(2)}\right\}$ included in N - $\left\{n_j^{(0)}\right\}$ - $\left\{n_j^{(1)}\right\}$ such that $\sum_j \left|a_{\beta^{(2)}\left(n_j^{(2)}\right)}\right| = y_2$. It should now be clear that our result follows by a simple induction on k.

References

1. Riemann series Theorem, https://en.wikipidia.org/wiki/Riemann_series_Theorem.
2. R. Fournier and J.M. Giguère, *On universality of series in Banach spaces*, CRM Proc. Lecture Notes, 55, A.M.S.(2012), 217-223.
3. R. Fournier and B. Ruffolo, *On divergent series with positive terms*, Dawson Research Journal of Experimental Science, V 13 (2018).

On the Series $\sum_{n=0}^{\infty}\left(-1\right)^{n} / \left(kn+1\right)$

Richard Fournier, Jonathan A. R. Halimi and Dragos Secrieru

Abstract

Given a positive integer k and k angles $\theta_j = (2j-1)\pi/k$, $j = 1, \ldots k$, we prove that

$$\sum_{n=0}^{\infty}\left(-1\right)^{n} / \left(kn+1\right) = -\frac{1}{k}\sum_{j=1}^{k}\cos\left(\theta_j\right)\ln\left\{2\sin\left(\frac{\theta_j}{2}\right)\right\} + \sin\left(\theta_j\right)\left(\theta_j - \pi\right)/2 \quad .$$

``*Entre deux vérités du monde réel, le chemin le plus facile et le plus court passe bien souvent par le domaine complexe*``

Paul Painlevé, 1900

Introduction

In this note we intend to present several ideas for the computation of the series $s_k = \sum_{n=0}^{\infty}\left(-1\right)^{n} / \left(kn+1\right)$ when k is a positive integer. We shall use a mixture of real and complex analysis to achieve our goal. The above series are convergent by test of Leibniz (sometimes called the alternating series test), however not absolutely convergent; it is for example known that certainly

$$s_1 = \ln\left(2\right), s_2 = \frac{\pi}{4}, s_3 = \frac{\ln\left(2\right)}{3} + \sqrt{3}\pi / 9$$

and a gifted Calculus II student may even compute $s_4 = \dfrac{\sqrt{2}\ln\left(3+2\sqrt{2}\right)}{8} + \sqrt{2}\pi / 8$. We shall derive a general formula for s_k that covers all the seemingly unrelated values of the series for all $k \geq 1$.

Part 1 (Complex Analysis)

This is a topic slightly beyond the cegep mathematics curriculum but accessible to any student with decent background in Calculus. We refer to [1] for a mild introduction to complex analysis. The complex numbers

$$w_j = e^{i\left(2j+1\right)\pi/k} = \cos\left(\frac{\left(2j+1\right)\pi}{k}\right) + i\sin\left(\frac{\left(2j+1\right)\pi}{k}\right), \quad 1 \leq j \leq k \ ,$$

are all distinct and they are called the k -roots of -1 because they are indeed the complex zeros of the polynomial $p(x) = x^k + 1$. Let us consider

$$P\left(x\right) = \left(\frac{1}{k}\right)\sum_{j=1}^{k}\frac{p\left(x\right)}{1-\overline{w}_j x} = \left(\frac{1}{k}\right)\sum_{j=1}^{k}\frac{1+x^k}{1-\overline{w}_j x} = \left(\frac{1}{k}\right)\sum_{j=1}^{k}\frac{1-\left(\overline{w}_j x\right)^k}{1-\overline{w}_j x}$$

By the factor theorem, P is a polynomial of degree less or equal to $k-1$ such that for all $1 \leq j \leq k$,

$$P\left(w_j\right) = \lim_{x\to w_j}\left(\frac{1}{k}\right)\frac{1-\left(\overline{w}_j x\right)^k}{1-\overline{w}_j x} = \lim_{x\to w_j}\left(\frac{1}{k}\right)\sum_{l=0}^{k-1}\overline{w}_j^l x^l = \left(\frac{1}{k}\right)\sum_{l=0}^{k-1}\overline{w}_j^l w_j^l = 1$$

This means of course that the polynomial $P-1$ also of degree $\leq k-1$ has k distinct zeros and by the Fundamental Theorem of Algebra, P is identically equal to 1, that is

$$\frac{1}{1+x^k} = \left(\frac{1}{k}\right)\sum_{j=1}^{k}\frac{1}{1-\overline{w}_j x} = \sum_{n=0}^{\infty}\left(-1\right)^{n} x^{kn}$$

for all complex numbers x with $\left|x\right| < 1$ and in particular for all reals $x \in [0, 1)$. Upon integration we find that

$$\int_0^x 1/\left(1+t^k\right)dt = \left(\frac{1}{k}\right)\sum_{j=1}^{k} -w_j \ln\left(1-\overline{w}_j x\right) = \sum_{n=0}^{\infty}\left(-1\right)^{n}\frac{x^{kn+1}}{kn+1}$$

and by the famous Theorem of Abel [2],

$$\sum_{n=0}^{\infty}\left(-1\right)^{n} / \left(kn+1\right) = \operatorname*{Lim}_{x\to 1^{-}}\sum_{n=0}^{\infty}\left(-1\right)^{n}\frac{x^{kn+1}}{kn+1} = \left(\frac{1}{k}\right)\sum_{j=1}^{k} -w_j \ln\left(1-\overline{w}_j\right) = \int_0^1 \frac{dt}{1+t^k}$$

where in the last step we have used the fact that for all $x \in [0, 1)$

$$\left|\int_0^x \frac{dt}{1+t^k} - \int_0^1 \frac{dt}{1+t^k}\right| = \int_x^1 \frac{dt}{1+t^k} \leq 1-x$$

Moreover, because the values of each of our series is a real number, we also have the representation

$$\left(\frac{1}{k}\right)\sum_{j=1}^{k} -\overline{w}_j \ln\left(1-w_j\right) = \sum_{n=0}^{\infty}\left(-1\right)^{n} / \left(kn+1\right) = \left(\frac{1}{k}\right)\sum_{j=1}^{k} -\ln\left(1-w_j\right) / w_j$$

for each $k \geq 1$. We shall use the following formula for the complex logarithm, valid for all $\theta \in (0, 2\pi)$,

Part 1 (Complex Analysis)

This is a topic slightly beyond the cegep mathematics curriculum but accessible to any student with decent background in Calculus. We refer to [1] for a mild introduction to complex analysis. The complex numbers

$$w_j = e^{i(2j+1)\pi/k} = \cos\left(\frac{(2j+1)\pi}{k}\right) + i\sin\left(\frac{(2j+1)\pi}{k}\right), \quad 1 \le j \le k \ ,$$

are all distinct and they are called the k -roots of -1 because they are indeed the complex zeros of the polynomial $p(x) = x^k + 1$. Let us consider

$$P(x) = \left(\frac{1}{k}\right)\sum_{j=1}^{k} \frac{p(x)}{1-\overline{w}_j x} = \left(\frac{1}{k}\right)\sum_{j=1}^{k} \frac{1+x^k}{1-\overline{w}_j x}$$
$$= \left(\frac{1}{k}\right)\sum_{j=1}^{k} \frac{1-(\overline{w}_j x)^k}{1-\overline{w}_j x}$$

By the factor theorem, P is a polynomial of degree less or equal to $k-1$ such that for all $1 \le j \le k$,

$$P(w_j) = \lim_{x\to w_j}\left(\frac{1}{k}\right)\frac{1-(\overline{w}_j x)^k}{1-\overline{w}_j x} = \lim_{x\to w_j}\left(\frac{1}{k}\right)\sum_{l=0}^{k-1}\overline{w}_j^l x^l$$
$$= \left(\frac{1}{k}\right)\sum_{l=0}^{k-1}\overline{w}_j^l w_j^l = 1$$

This means of course that the polynomial $P-1$ also of degree $\le k-1$ has k distinct zeros and by the Fundamental Theorem of Algebra, P is identically equal to 1, that is

$$\frac{1}{1+x^k} = \left(\frac{1}{k}\right)\sum_{j=1}^{k}\frac{1}{1-\overline{w}_j x} = \sum_{n=0}^{\infty}(-1)^n x^{kn}$$

for all complex numbers x with $|x| < 1$ and in particular for all reals $x \in [0, 1)$. Upon integration we find that

$$\int_0^x 1/(1+t^k)\,dt = \left(\frac{1}{k}\right)\sum_{j=1}^{k} -w_j \ln(1-\overline{w}_j x)$$
$$= \sum_{n=0}^{\infty}(-1)^n \frac{x^{kn+1}}{kn+1}$$

and by the famous Theorem of Abel [2],

$$\sum_{n=0}^{\infty}(-1)^n/(kn+1) = \operatorname*{Lim}_{x\to 1^-}\sum_{n=0}^{\infty}(-1)^n\frac{x^{kn+1}}{kn+1}$$
$$= \left(\frac{1}{k}\right)\sum_{j=1}^{k} -w_j\ln(1-\overline{w}_j)$$
$$= \int_0^1 \frac{dt}{1+t^k}$$

where in the last step we have used the fact that for all $x \in [0, 1)$

$$\left|\int_0^x \frac{dt}{1+t^k} - \int_0^1 \frac{dt}{1+t^k}\right| = \int_x^1 \frac{dt}{1+t^k} \le 1-x$$

Moreover, because the values of each of our series is a real number, we also have the representation

$$\left(\frac{1}{k}\right)\sum_{j=1}^{k} -\overline{w}_j\ln(1-w_j) = \sum_{n=0}^{\infty}(-1)^n/(kn+1)$$
$$= \left(\frac{1}{k}\right)\sum_{j=1}^{k} -\ln(1-w_j)/w_j$$

for each $k \ge 1$. We shall use the following formula for the complex logarithm, valid for all $\theta \in (0, 2\pi)$,

$$\ln(1-e^{1\theta}) = \ln|1-e^{1\theta}| + iArg(1-e^{1\theta})$$
$$= \ln\left\{2\sin\left(\frac{\theta}{2}\right)\right\} + i\,\frac{\theta-\pi}{2}$$

and we conclude that.

$$s_k = \left(-\frac{1}{k}\right)\sum_{j=1}^{k}\operatorname{Re}\left\{\overline{w}_j\ln(1-w_j)\right\}$$
$$= \left(-\frac{1}{k}\right)\sum_{j=1}^{k}\operatorname{Re} w_j \operatorname{Re}\left\{\ln(1-w_j)\right\} + \operatorname{Im} w_j \operatorname{Im}\left\{\ln(1-w_j)\right\}$$

Finally

$$s_k = \left(-\frac{1}{k}\right)\sum_{j=1}^{k}\cos\left(\frac{(2j-1)\pi}{k}\right)\ln\left\{2\sin\left(\frac{(2j-1)\pi}{2k}\right)\right\} + \sin\left(\frac{(2j-1)\pi}{k}\right)\left\{\frac{(2j-1)\pi}{2k} - \frac{\pi}{2}\right\}.$$

The doubtful reader may check that this last formula coincides with the values given above for s_k for small values of k.

Part 2 (Real Analysis)

In this section we first show how to use Calculus II methods to derive the above identity when k is even; in that case, the k -roots of -1 come by conjugate pairs and we have for x real,

$$\frac{1}{1+x^k} = \left(\frac{1}{k}\right)\sum_{j=1}^{k/2}\frac{1}{1-w_j x} + \frac{1}{1-\overline{w}_j x}\,.$$

Of course, this yields the usual representation into partial fractions

$$\frac{1}{1+x^k} = \frac{1}{k}\sum_{j=1}^{k/2}\left\{\frac{2-2\operatorname{Re}(w_j)x}{1-2\operatorname{Re}(w_j)x+x^2}\right\}$$

because the quadratic "factors" $\{1-2\mathrm{Re}(w_j)x+x^2\}$ are all irreducible. The rest is just business as usual. We first obtain

$$\frac{1}{1+x^k}=\left(\frac{1}{k}\right)\sum_{j=1}^{k/2}-\operatorname{Re}\left(w_j\right)\frac{2x-2\operatorname{Re}\left(w_j\right)}{1-2\operatorname{Re}\left(w_j\right)x+x^2}$$
$$+\left(\frac{2}{k}\right)\sum_{j=1}^{k/2}1\Big/\left\{1+\left[\frac{x-\operatorname{Re}\left(w_j\right)}{\sqrt{1-\operatorname{Re}^2\left(w_j\right)}}\right]^2\right\}$$

and integrating the last identity yields $s_k = s_{k,1} + s_{k,2}$ where

$$s_{k,1}=\left(\frac{1}{k}\right)\sum_{j=1}^{k/2}-\operatorname{Re}\left(w_j\right)\ln\left\{2-2\operatorname{Re}\left(w_j\right)\right\}$$
$$=\left(\frac{1}{2k}\right)\sum_{j=1}^{k}-\operatorname{Re}\left(w_j\right)\ln\left\{2-2\operatorname{Re}\left(w_j\right)\right\}$$

which leads to

$$s_{k,1}=\left(-\frac{1}{k}\right)\sum_{j=1}^{k}\operatorname{Re}\left(w_j\right)\ln\left|1-w_j\right|,$$

while we may write together with

$$c_j=2\sin\left(\theta_j\right)\left\{\arctan\left[\tan\left(\frac{\theta_j}{2}\right)\right]+\arctan\left[\cot\left(\theta_j\right)\right]\right\}$$

$$s_{k,2}=\left(\frac{1}{k}\right)\sum_{j\le\left(\frac{k}{2}+1\right)/2}c_j+\left(\frac{1}{k}\right)\sum_{j>\left(\frac{k}{2}+1\right)/2}c_j.$$

These two last sums can be seen to amount to

$$\left(\frac{1}{k}\right)\sum_{j\le\left(\frac{k}{2}+1\right)/2}2\sin\left(\theta_j\right)\left(\frac{\theta_j}{2}+\frac{\pi}{2}-\theta_j\right)$$
$$+\left(\frac{1}{k}\right)\sum_{j.>\left(\frac{k}{2}+1\right)/2}2\sin\left(\theta_j\right)\left(\frac{\theta_j}{2}-\frac{\pi}{2}+\pi-\theta_j\right).$$

A bit more work shows that this last quantity is simply

$$s_{k,2}=\left(-\frac{1}{k}\right)\sum_{j=1}^{k/2}2\sin\left(\theta_j\right)\left(\frac{\theta_j}{2}-\frac{\pi}{2}\right)$$
$$=\left(-\frac{1}{k}\right)\sum_{j=1}^{k}\sin\left(\theta_j\right)\left(\frac{\theta_j}{2}-\frac{\pi}{2}\right)$$

which indicates that our result here coincides with what was obtained in Part 1. In the case where k is odd, we have

$$\frac{1}{1+x^k}=\left(\frac{1}{k}\right)\sum_{j=1}^{k}\frac{1}{1-\bar{w}_j x}$$
$$=\left(\frac{1}{k}\right)\frac{1}{1+x}+\left(\frac{1}{k}\right)\sum_{j=1}^{(k-1)/2}\frac{1}{1-w_j x}+\frac{1}{1-\bar{w}_j x}.$$

Integrating over $[0,\ 1]$, we get $s_k = s_{k,1} + s_{k,2}$ where

$$s_{k,1}=\left(\frac{1}{k}\right)\ln\left(2\right)+\left(-\frac{1}{k}\right)\sum_{j=1}^{(k-1)/2}\operatorname{Re}\left(w_j\right)\ln\left\{2-2\operatorname{Re}\left(w_j\right)\right\}$$

that is

$$s_{k,1}=\left(\frac{1}{k}\right)\ln\left(2\right)+\left(-\frac{2}{k}\right)\sum_{j=1}^{(k-1)/2}\operatorname{Re}\left(w_j\right)\ln\left|1-w_j\right|$$
$$=\left(-\frac{1}{k}\right)\sum_{j=1}^{k}\operatorname{Re}\left(w_j\right)\ln\left|1-w_j\right|.$$

We evidently also have

$$s_{k,2}=\left(-\frac{1}{k}\right)\sum_{j=1}^{k}\operatorname{Im}\left(w_j\right)\operatorname{Im}\left\{\ln\left(1-w_j\right)\right\}$$

where we have made use of the fact that $\operatorname{Im}\{\ln(1-w)\}$ is bounded when $|w|=1$.

References

1. Complex number in Wikipedia, https://en.wikipedia.org/wiki/Complex_number
2. Abel's theorem in Wikipedia: https://en.wikipedia.org/wiki/Abel%27stheorem
3. Concerning the very busy life of Painlevé, the interested reader may consult https://en.wikipedia.org/wiki/Paul_Painlevé

About Dr Jes

The Dawson Research Journal of Experimental Science (DrJes) is a student publication of Dawson College's Science Program. Its aim is to publish experimental research undertaken by college students, either independently or as part of their program of study, to increase their familiarity with the scientific method. Subscriptions are available at cost plus postage and handling. Advertising matters, subscriptions, changes of address, and submission should all be forwarded to the mailing address provided below. For further information, please visit the DrJes webpage.

Contact

Mailing Address
The Dawson Research Journal of Experimental Science (DrJes)
Suite 6B.17-1 (c/o Brid Nic Niocaill)
3040 Sherbrooke
Montreal QC H3Z 1A4
Canada

E-mail
Brid NicNiocaill (Faculty Editor): bnicniocaill@dawsoncollege.qc.ca
Webmaster: drjes@dawsoncollege.qc.ca